State of Delaware
DELAWARE GEOLOGICAL SURVEY
David R. Wunsch, State Geologist

# BULLETIN NO. 21B

# HYDROGEOLOGY OF A RAPID INFILTRATION BASIN SYSTEM (RIBS) AT CAPE HENLOPEN STATE PARK, DELAWARE

By

Scott Andres[1], Edward Walther[2],
Müserref Türkmen[3], Changming He[1]

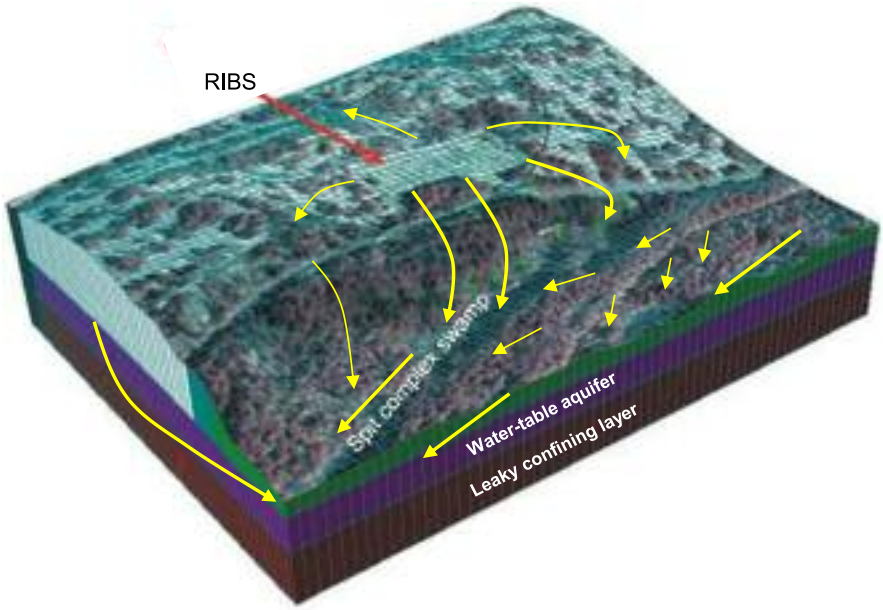


Delaware Geological Survey
University of Delaware
Newark, Delaware
2015

[1] Delaware Geological Survey
[2] South Florida Water Management District, West Palm Beach, Florida
[3] Izmir Water and Sewerage Administration, Izmir, Turkey

# TABLE OF CONTENTS

## ILLUSTRATIONS

Page



## TABLES



## APPENDICES

# HYDROGEOLOGY OF A RAPID INFILTRATION BASIN SYSTEM (RIBS) AT CAPE HENLOPEN STATE PARK, DELAWARE


## ABSTRACT

The hydrogeologic framework of Cape Henlopen State Park (CHSP), Delaware was characterized to document the hydrologic effects of treated wastewater disposal on a rapid infiltration basin system (RIBS). Characterization efforts included installation of test borings and monitoring wells; collection of core samples, geophysical logs, hydraulic test data, groundwater levels and temperatures; testing of grain size distribution; and interpretation of stratigraphic lithofacies, hydraulic test data, groundwater levels, and temperature data. This work was part of a larger effort to assess the potential benefits and risks of using RIBS in Delaware.

The infiltration basins at CHSP are constructed on the Great Dune, an aeolian dune feature composed of relatively uniform, medium-grained quartz sand. The age of the dune, determined by carbon-14 dating of woody material in swamp deposits under the dune, is less than 800 years. Underlying the dune deposits are relatively heterogeneous, areally continuous, coarse-grained spit deposits of the proto-Cape Henlopen spit with interbedded and relatively fine-grained, discontinuous swamp and marsh deposits, and beneath, relatively fine-grained, continuous, near-shore marine deposits. The dune deposits can be 45 ft thick under the crest of the dune and nonexistent at the surface. Spit deposits range from 5 to 15 ft thick. Test drilling determined that the near-shore marine deposits are at least 10 ft thick in the vicinity of the infiltration basins. The complete thickness of these deposits was not determined in this study.

Hydraulic testing and grain-size data indicate that the dune and spit deposits are relatively permeable, with average hydraulic conductivities of 140 ft/day and that the swamp and marsh deposits are more than one order of magnitude less permeable, with average hydraulic conductivity of 25 to 10 ft/day. The water-table aquifer is present in the sandier dune and spit deposits. The swamp, marsh, and near-shore marine deposits form a leaky confining unit. The water-table aquifer is 15 to 20 ft thick under the thickest section of the Great Dune and nonexistent where the dune deposits are absent. The vadose zone is greater than 25 ft thick under the infiltration basins.

High-frequency groundwater level and temperature monitoring during periods of maximum wastewater disposal rates indicates that wastewater disposal causes increases in water-table elevations on the order of 1 ft. Groundwater elevations indicate that the water-table elevation is greatest under the infiltration basins and that most flow is directed southward toward a swampy discharge area.

Maximum disposal rates typically occur in summer months when the numbers of park users and water use are greatest. Coincident with greater disposal rates are higher wastewater temperatures. These higher wastewater temperatures are observed in groundwater and provide a means to track the flow of water from beneath the infiltration beds towards a nearby discharge area. Tracking of the warmer groundwater and modeling two-dimensional particle tracking both indicate that wastewater discharged to the infiltration basins reaches the nearby discharge area within 180 days.


## INTRODUCTION

Rapid infiltration basin systems (RIBS) utilize several simple and relatively standard technologies for the land-based disposal of wastewater. In Delaware, wastewater collected from parks, homes, and businesses is conveyed to a treatment plant where it undergoes chemical, biological, and physical processing. The effluent is then discharged to an unlined excavated or constructed basin where it quickly infiltrates through the unsaturated (vadose) zone to the water table. Once in the aquifer, much of the effluent will eventually discharge into a body of surface water. Depending on the location and design characteristics of an individual RIBS, the effluent may be intercepted and pumped by water supply wells, or portions of the effluent may slowly percolate deeper into the aquifer or into the underlying confined aquifers.

If all of the individual components of a RIBS are working properly, the water may be safely reclaimed for other purposes, such as maintaining surface water flow, sustaining important subaqueous and wetland habitats, and supplying water for non-potable or even potable uses. However, nearly 40 years of research by academic, state, and federal scientists have documented that the Columbia aquifer beneath Delaware is highly susceptible to contamination when wastes are applied onto and into the ground. Contaminants persist in the groundwater for decades, impacting potable water supply wells, and discharging into surface water bodies, leading to the well-documented eutrophication problems (Miller, 1972; Robertson, 1977; Ritter and Chirnside, 1982, 1984; Andres, 1991; Guitierrez-Magness and Raffensperger, 2003; Denver et al., 2004; Pellerito et al., 2006). Debrewer et al. (2005) and Ator (2008) found that the causes of Delaware's water quality problems are consistent with those observed throughout the Delmarva Peninsula and much of the Mid-Atlantic Coastal Plain. As a result, when one or more of the components of a RIBS malfunction, or if there are negative, unanticipated natural hydraulic and/or geochemical factors, there is a substantial risk for the effluent to adversely impact sensitive public (water supply wells) and environmental (streams, wetlands) receptors.

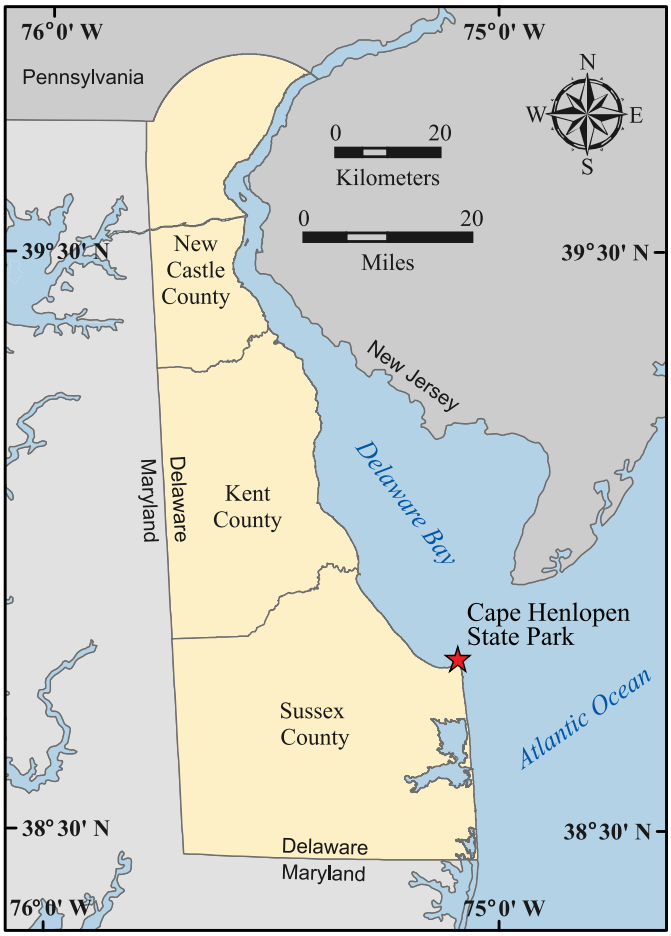


**Figure 1.** General location map.

### Purpose and Scope

This report covers the physical hydrogeological component of the second phase of a multi-year, multi-disciplinary project to systematically analyze the results and the risks associated with the operation of RIBS in Delaware. The first phase was an evaluation of wastewater treatment options used in RIBS, and is documented in Delaware Geological Survey (DGS) Bulletin 21A (Türkmen et al., 2015). During the second phase, we have conducted a variety of field experiments to characterize the geology and hydrogeology of a RIBS facility at Cape Henlopen State Park (CHSP, Fig. 1) and the physical hydrogeological affects on shallow groundwater that are caused by the addition of treated sewage effluent through rapid infiltration beds.

### Acknowledgments

This work was funded by the Delaware Department of Natural Resources and Environmental Control (DNREC) and the DGS. We thank Patrick Boetcher, Joshua Kasper, and Scott Strohmeier (DNREC), Steve McCreary, Thomas McKenna, and Jaime Tomlinson (DGS), and Janine Howard, Ashley Beers, Justin Wagner, Jennalee Rufft, Curt Romanchock, Ian McCann, and Holly Michael (University of Delaware) for their participation in the field work. The Delaware Division of Air and Waste Management provided a Geoprobe rig equipped with a single barrel coring device and operator (Patrick Boettcher) for three days. We especially thank the DNREC Division of Parks and Recreation and the staff of CHSP for permission to access property and for their assistance with logistics. Steven Smailer of Duffield Associates and John Barndt and Scott Strohmeier of the DNREC Water Supply Section critically reviewed the manuscript.

## METHODS

Subsurface materials were characterized by analysis of samples and measurements collected from test borings, direct push coring, downhole geophysical logging, monitoring wells, and subsurface hydraulics data. Analyses of soils and sediments included visual descriptions, grain size distributions, and water content data. Hydraulics testing included single-well aquifer tests (slug tests), ring infiltrometer tests, and groundwater-level measurements. The locations of the observation points are shown on Figures 2 and 3. Site identifiers shown on Figure 2 are indexed to wells listed in Appendix A1.

### Field Methods for Characterization of Soils, Sediments, and Water

The locations for observations within the infiltration basins were chosen based on 2007-edition high resolution, georeferenced aerial photography (http://datamil.delaware.gov; accessed in 2009) in conjunction with the facility's engineering drawings. Locations for observations outside of this area were determined using a real-time corrected global positioning system.

During February 2008, two 25-ft borings and eight 10-ft borings were completed using a Geoprobe rig equipped with a single barrel coring device (Fig. 2). Core samples were collected within standard acetate core barrel liners, which were opened in the field, visually inspected, and photographed. Material sloughed from the side of the hole was discarded. The core samples were cut into 2-ft lengths, photographed, placed in core boxes, covered with polyethylene film, and transported to the DGS laboratory, where they were split with a mechanical splitter; one portion was saved for particle size analysis and the other portion was used for chemical analysis.

In February and March 2008, two 2-ft deep hand auger borings were made in each of the eight infiltration beds (Fig. 3). One boring in each bed was completed in a vegetated area near a wastewater discharge head, and another was completed in a non-vegetated area. Separate samples were collected from 0 to 1 ft and 1 to 2 ft below the surface. Samples were split with a mechanical splitter; one portion was saved for particle size analysis and the other portion was used for chemical analysis.

Test borings were completed and monitoring wells were installed at nine locations using the DGS CME-55 drill rig and at five locations using a hand auger (Figs. 2, 3). Split-spoon core samples and downhole natural gamma radiation logs were collected through the annulus of the 2-1/4 inch inside diameter (ID) augers at Ni45-33 and Ni45-35. The core samples were described in detail on site and compared with the gamma logs to develop a model of site stratigraphy and hydrostratigraphy, and to design well screen settings at all well sites. Several of the core samples were later sub-sampled for chemical testing.

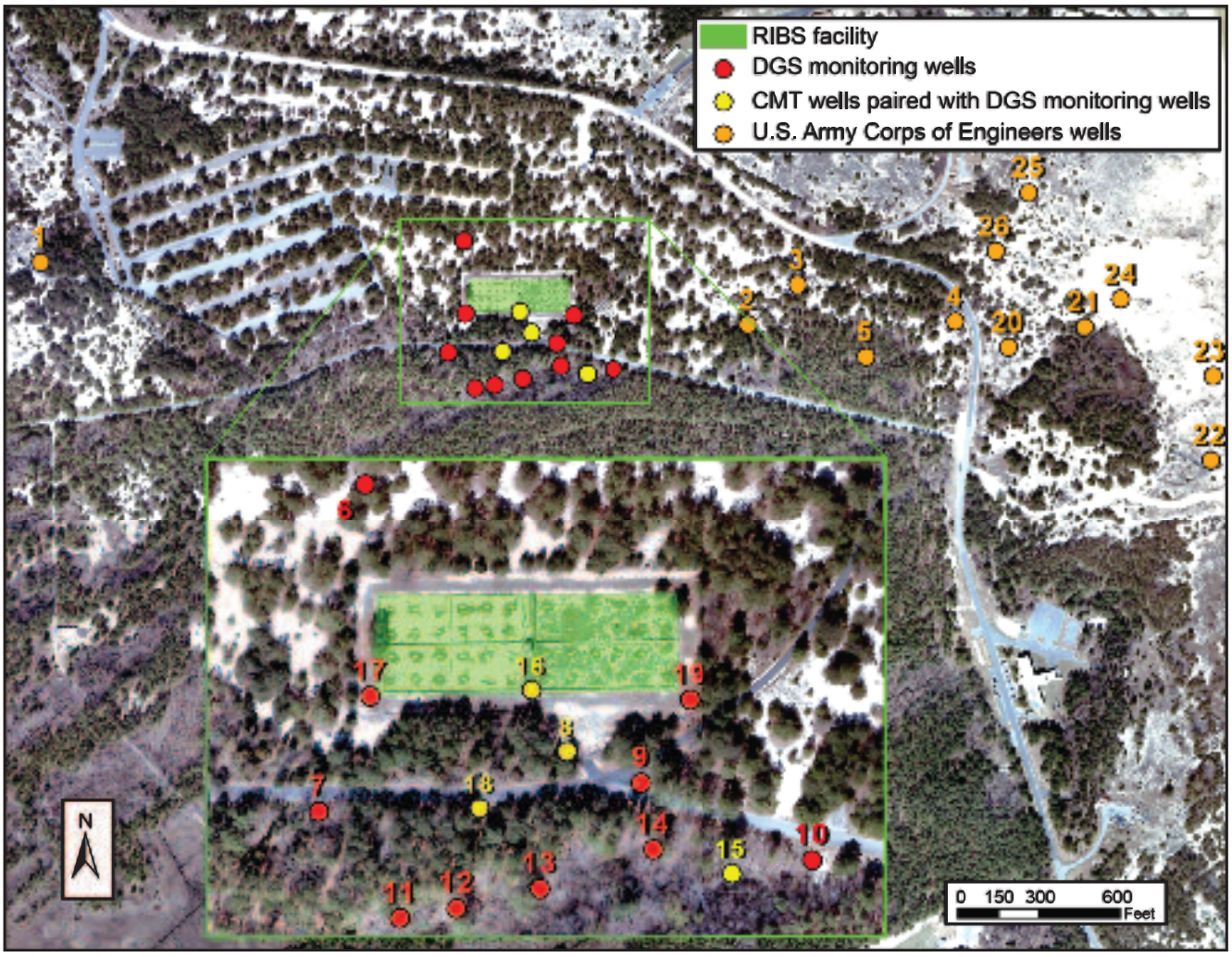


**Figure 2.** Locations of monitoring wells. CMT refers to Solinst CMT multi-port monitoring device. Site identification numbers are indexed to wells listed in Appendix A1.

Standard monitoring wells consisting of 2-inch ID threaded flush joint schedule 40 PVC pipe connected to machine slotted schedule 40 PVC well screen were installed. Wells installed in holes drilled by the truck-mounted equipment had 15 ft of machine-slotted well screen. Wells installed by hand augering had 3 ft of machine-slotted well screen. All wells were gravel packed and grouted with granular sodium bentonite, with the gravel pack extending at least 1 ft above the top of the screen interval. Grout was emplaced by tremie pipe in the machine-drilled holes and by hand in the hand augered holes. All of the wells that were located in easily accessible areas were covered with protective steel casings embedded in concrete pads.

Consultants for the U.S. Army Corps of Engineers installed wells during multiple subsurface investigations, one in the 1990s (US Army Corps of Engineers, 1997), and another in November and December 2008 (James Stuby, written communication). Four of the wells from the 1990s were monitored for this study (Fig. 2). Seven temporary 2-inch ID monitoring wells were installed in 2008 (Fig. 2); water levels were measured in these wells during December 2008.

Natural gamma-induction electric logs were run in all of the wells installed with the CME rig. Geophysical logs and visual descriptions from samples of drill cuttings were used to refine the interpretations of hydrostratigraphy developed from the cored test borings.

Four 7-channel multi-level wells (CMT System - Solinst Canada) were installed next to the standard wells at four locations (Fig. 2). The depths of the individual sample ports were determined from an analysis of the descriptive and geophysical logs collected at the same site. Gravel pack was emplaced to span the interval between 2 ft above the top sample port to the bottom of the CMT tube. Grout was emplaced with a tremie pipe from the top of the gravel pack to within a few feet of the land surface. Protective casings embedded in 2-ft thick concrete or bentonite plugs were placed over all CMT wells.

*Moisture content of vadose zone*

Ten additional split-spoon test borings for determining gravimetric (Wg) and volumetric water contents (Vw), and constructing time domain reflectometry (TDR) moisture profiling tubes (MPT) were completed within the infiltration basins (Fig. 3). At each location, hand tools (slide hammer, tripod, and winch) were used to drive and retrieve a standard split-spoon sampling device with an acetate liner. To sample a known volume of material, the split spoon was advanced

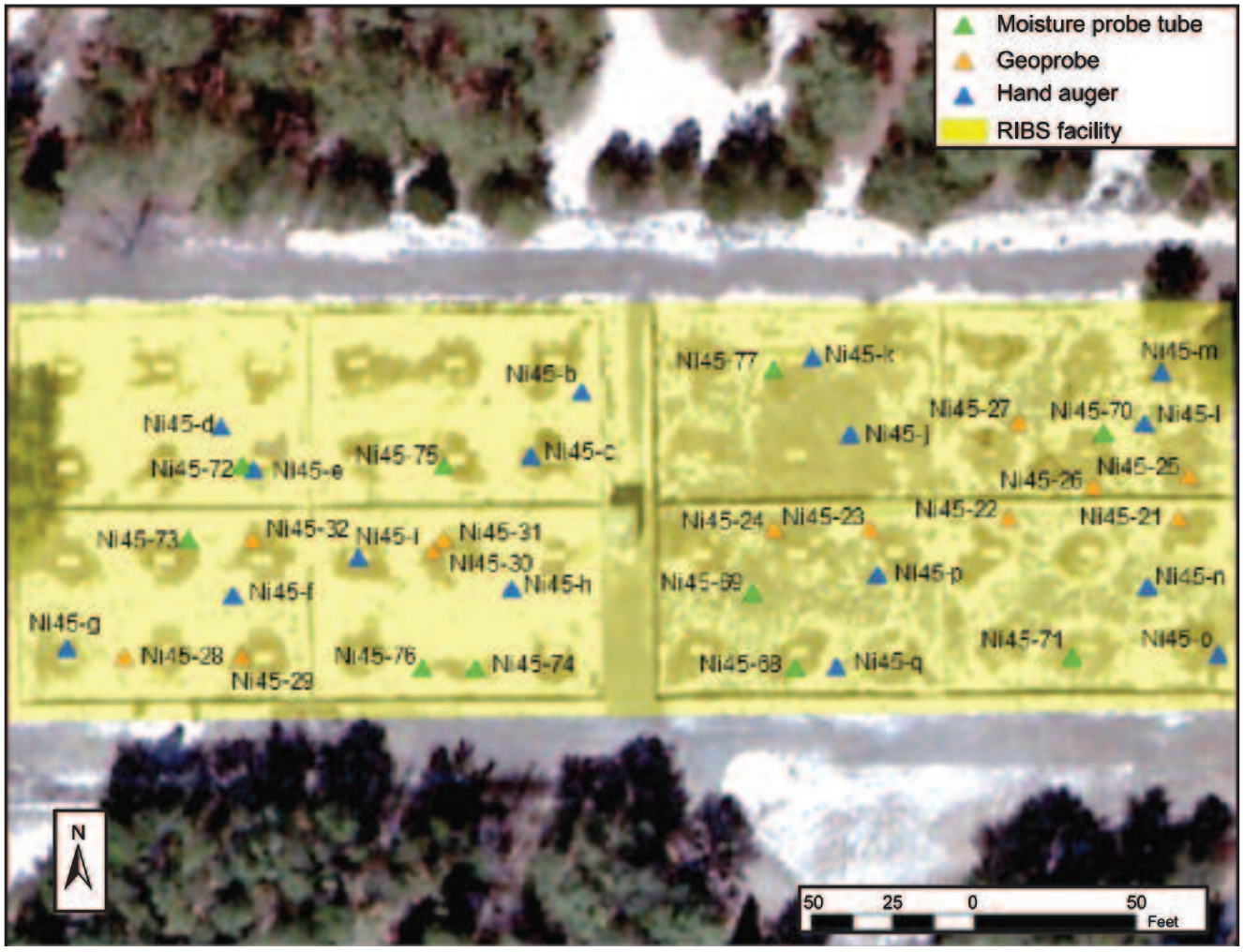


**Figure 3.** Locations of test borings and moisture profiling tubes.

1 ft and then removed from the hole. The cores were inspected and any portion of the core containing material sloughed from the side of the hole was discarded. The samples were then capped and transported back to the DGS building for a determination of grain size distribution and gravimetric moisture content, and for the computation of volumetric moisture content (Vw) and porosity (n).

Each MPT constructed in the split-spoon holes described in the preceding paragraph consists of a 2-inch ID schedule 40 PVC pipe with bottom end plug and top slip cap. Because the diameter of the MPT is larger than the split spoon sampler, the sampler holes were enlarged by inserting and removing a 2-inch ID schedule 40 galvanized steel pipe. This process allowed for close coupling of the MPTs and the surrounding material.

In-situ Vw was monitored with a Trime FM tube-type TDR that was inserted into the MPT to a predetermined depth; the electronics were then activated, and depth and Vw were recorded. The instrument was factory calibrated in July 2008 and November 2008. Calibration was conducted in the field at the beginning of each day and consisted of activating the instrument with the probe in free air to ensure that the instrument would return the expected 0 percent moisture value. A detailed description of the principles of TDR operations is in Robinson et al. (2003) and Laurent et al. (2005). These measurements were collected to estimate irreducible water content (Vw0), saturated water content (VWs), and effective porosity (ne). Bear (1979) defines irreducible Vw0 as the proportion of water (relative to total volume, Vt) that is immobilized by capillary forces or in dead-end pores. Similarly, ne is the difference between n and Vw0, and VWs is equivalent to n.

*Groundwater measurements*

Groundwater levels were measured manually to the nearest 0.01 ft with Solinst electric water-level meters and automatically with In-Situ, Inc. transducer/data logger instruments. Barometric pressure data were collected on site with an In-Situ, Inc. barometer. For periods when the barometer was inoperable, barometric pressure data were collected at the Delaware Environmental Observation System (DEOS) station located approximately 3 miles to the south in Rehoboth Beach, Delaware. Barometric corrections were computed with In-Situ Baromerge software or, in the case of the DEOS data, in an electronic spreadsheet. Quality assurance/quality control (QA/QC) procedures for the automated data were conducted following the manufacturer's guidance and internal DGS procedures. All data were archived in DGS internal databases.

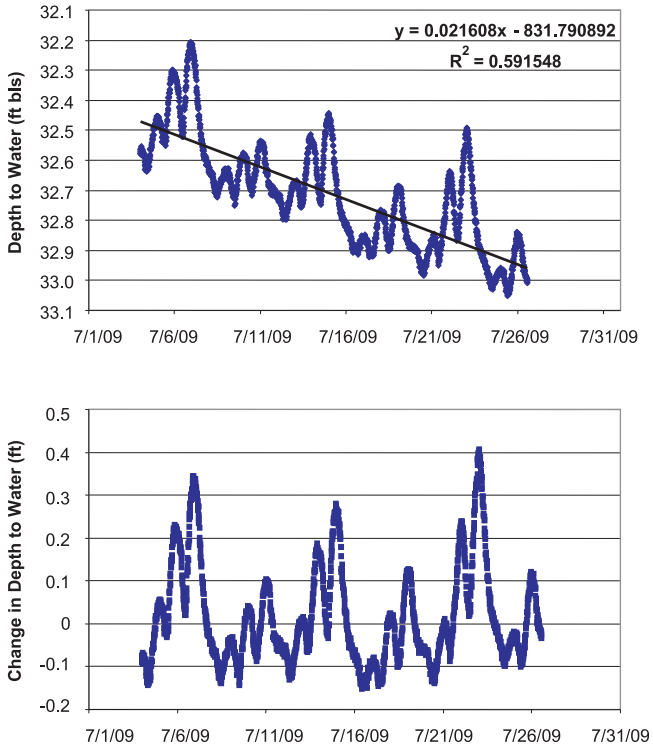


**Figure 4.** Illustration of raw (top) and detrended (bottom) water-level records. Example is from well Ni45-43.

The analysis of small changes in water level required subtracting long-term trends (i.e., declines and increases) from the raw data (Fig. 4). In these cases, the analysis consisted of linear regression analysis followed by calculation of residuals.

*Hydraulic testing*

Slug tests were conducted and results were analyzed using the guidelines established in Butler (1996). Because the well screens spanned the water table, water was displaced with a mechanical slug constructed of a sand-filled 0.75-inch ID capped, PVC pipe. Insertion and retrieval of the slug were controlled with a nylon cord. Within each 2-inch ID monitoring well, at least three rising head tests were conducted with an In-Situ, Inc. transducer/data logger that was used in conjunction with the manufacturer's software for instrument control and data capture. Data analysis was conducted using the Bouwer and Rice (Bouwer, 1989) method and Aquifer Test Pro software (Schlumberger Water Systems, 2008).

Several types of infiltration tests were conducted in the infiltration basins at the sites of the MPTs to measure the apparent saturated vertical hydraulic conductivity. Double ring infiltrometer experiments were conducted by a method that is functionally equivalent to ASTM D3385 (ASTM, 2003). The data from these tests provide an estimate of apparent saturated vertical hydraulic conductivity. Data loggers in the inner and outer rings recorded head at 2-second intervals. Two 40-gallon tanks were used as reservoirs and water was delivered to the rings via valve controlled hoses. (Mariotte tubes could not deliver the necessary water because of the high permeability of the infiltration surface and the difficulty of moving large water reservoirs across the soft sandy surface of the basins.) The valves were adjusted to maintain head in the rings as close to 1 ft as possible. The flow rate to the inner ring was determined from a time series of the height of water in a reservoir with a predetermined stage height – volume curve. Stage-height data were recorded by a data logger mounted in the reservoir. Downhole moisture content measurements were made during each infiltration test in an MPT with the TRIME-FM tube-TDR and recorded with a datalogger. Data from tests were processed in spreadsheets; infiltration rates were determined from periods for which flow rates and heads were held relatively constant. A more complete description of the test methods used on the site is available in Rufft, 2009.

### Laboratory Measurements of Physical Properties

Methods described in Kramer (1987) were used to determine the grain-size distribution of some samples (Appendix B1). Gravimetric water contents were determined on selected core samples. Sample weights were determined to the nearest 0.1 gram with an Ohaus E400 electronic scale and the total sample volume was estimated from the length of the sample and the inside diameter of the core barrel liner. The density of the solid phase was assumed to be 2.65 g/cc (e.g., quartz). Porosity, volumetric water content and bulk density were estimated for these samples using standard soil mechanics equations. Because the samples were loosely consolidated, determining sample length and computing volumetric water content and bulk density was problematic for some samples.

## RESULTS AND DISCUSSION

### Wastewater Treatment and Effluent Disposal

The wastewater treatment plant at the CHSP is a primary treatment system consisting of two Imhoff tanks constructed for the U.S. Army in 1941 (Lee McDaniel, personal communication). The plant treats water generated by a campground, a beach bath house, administrative and maintenance buildings, a visitor center, residences, and several dormitories that include food preparation facilities. Dormitories at CHSP are used by school groups during the school year and by several sports camps during the summer. The treatment plant is maintained by two CHSP employees who are State of Delaware licensed wastewater treatment plant operators. A detailed description of the plant is contained in Türkmen et al. (2008). Because the treatment plant has minimal storage capacity, effluent is discharged to the infiltration basins in doses having a frequency that depends on influent flow rates.

A small building located in the middle of the array of eight infiltration basins, or beds, contains a mechanical valve system with switches controlling the discharge of treated effluent between basins. The effluent discharge location changes roughly every day, from one basin to the next, following a clockwise pattern (Lee McDaniel, personal communication). On most weekdays, CHSP personnel record the cumulative effluent flow into each infiltration bed. However, our observations of effluent discharge locations did not match the records written by park personnel. We also observed that switching between beds did not happen at the

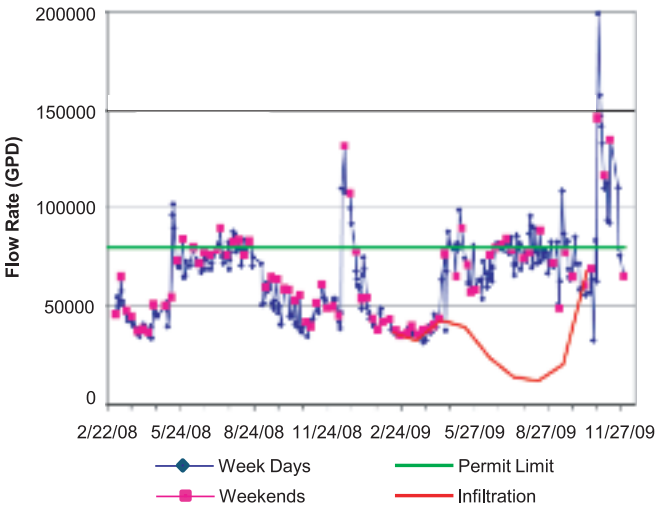


**Figure 5.** Reported daily effluent discharge from the park wastewater treatment plant in gallons per day (gpd). Infiltration calculated as the difference between monthly effluent flow and water purchase records. Flow reported in gpd. The permit limit of 80,000 gpd is an average monthly flow.

same time every day. To estimate weekend flows, we calculated the difference between flows recorded on Fridays and Mondays.

Average flow during the study was just over 65,000 gallons per day (gpd). Effluent disposal rates vary with the number of daily and overnight park visitors, which vary by season and day of the week. Not surprisingly, the greatest sewage flow occurs during summer months and on weekends when the number of visitors is the largest. Flow rates are ordinarily 10,000 to 15,000 gpd greater on summer weekends than on summer weekdays, and more than 20,000 gpd greater than in the off season. During much of the year, effluent disposal rates coincide with effluent temperatures, which range from a low of about 12°C in the winter to over 21°C in the summer. High temperatures appear to be correlated with the increased use of warm water at the bath house.

Effluent disposal rates also are affected by hydrologic conditions. Because portions of the sewage collection system consist of terra cotta pipe (Lee McDaniel, personal communication) there is substantial infiltration of groundwater into the collection system when the water table is high or when sections of the collection system fail. The excess water is processed in the treatment plant and discharged to the infiltration basins. A period of greater than normal effluent discharge was noted by park personnel in the winter and spring of 2008, which prompted repairs of the collection system (Lee McDaniel, personal communication). Differences between monthly effluent flow rates and monthly water purchase amounts in 2009 also indicate that there is infiltration of groundwater into the sewage collection system.

## Geologic Framework

Our understanding of the hydrogeology of the Cape Henlopen field site is from previous studies and our own observations made during drilling, water sampling, and visual observations. For this report, we mapped and described geologic units using the stratigraphic names and mapping model presented by Ramsey (2003), with interpretations of depositional environments assisted by Chadwick (2000). Leis (1974) conducted a hydrogeologic assessment of the general area including an investigation of aquifer hydraulics. We found that these previous works provided reasonable interpretations of the geology and hydrogeology of the site.

Geologic units encountered in the drilling program at CHSP are fill, unnamed Holocene dune deposits, unnamed Holocene swamp and marsh (herein named swamp/marsh) deposits, unnamed Holocene shoreline and spit deposits, and unnamed Holocene marine deposits (Figs. 6 and 7, Appendix A2). Chadwick (2000) found that the non-fill materials deposited in these environments exhibit complex interfingering and gradational facies changes over short lateral and vertical distances. Drilling did not intercept any deposits that could be positively identified as older Quaternary units (e.g., Lynch Heights or Scotts Corners Formations) or Tertiary units (e.g., Beaverdam or Bethany Formations).

### *Fill*

Over time, military and subsequent park personnel moved large quantities of material for use in road fill and military fortifications. Material identified as fill is predominately sand derived from the site; variable amounts of concrete, rebar, and crushed stone; and trace amounts of coal, paper, plastic, and metal foil. Exclusive of fill used in fortifications, the most significant accumulations of fill are located along the road (Fig. 2) and on the south facing slip face of the Great Dune.

### *Dune deposits*

Dune deposits are associated with the Great Dune and are predominately composed of sand with trace amounts of granules. These materials are generally shades of yellow and orange indicating oxidizing geochemical conditions. Dune deposits range in thickness from a featheredge at the toe of the dune to about 45 ft under the top of the dune. Grain size testing of 95 samples of dune deposits show that the sands are relatively uniform, with a mean grain size of 1.2 mm (range 0.68 - 1.62 mm) and a standard deviation of 0.57 (Appendix B1). Samples collected from the infiltration beds at depths less than 2 ft tend to be finer grained than samples from greater depths.

Porosities estimated from core samples range between 0.3 and 0.5 (Appendix B2) and are consistent with maximum Vw determined by TDR. Although these values are reasonable for the materials, difficulties with collecting and handling the cores may indicate that these estimates are not accurately quantifiable. TDR-measured ambient Vw collected during the autumn and winter at depths greater than 3-ft range from about 8.5 to 12 percent. Since these values were consistently observed following periods of limited precipitation at a time when no plants were growing, they likely represent Vw0. Effective porosity (ne) is the difference between n and Vw0 (Bear, 1979); our computed ne values

range between 0.28 and 0.41. The term ne is used for computing flow velocity (Bear, 1979).

Soils developed on the dune deposits are identified as the Acquango-Beaches complex, 0- to 10-percent slopes in the USDA Web Soil Survey (http://websoilsurvey.nrcs.usda.gov/app/WebSoilSurvey.aspx). In general, the uppermost 1 to 2 ft of this soil is composed of well-sorted, loose, medium-to fine-grained sands that are very pale yellow to very pale gray. Areas within the infiltration basins where effluent discharge has promoted plant growth have a soil profile containing more silt-sized material than in the non-vegetated areas or in undisturbed areas outside of the disposal area. The upper one ft of the profile commonly contains visible organic debris that ranges to up to 0.2 percent organic carbon, as determined by loss on ignition.

Natural gamma radiation (gamma) logs show that the dune deposits typically emit relatively low amounts of radiation, which is consistent with the quartzose sand composition. Electromagnetic conductance (EM) logs show that dune deposits give very low conductance readings when dry, but readings that are 2- to 5-times higher when wet.

*Spit deposits*

Spit deposits were left by the northward migration of proto-Cape Henlopen (Chadwick, 2000). These deposits form the northeast-southwest trending arcuate ridges located south of the Great Dune. Spit deposits are present south of the Great Dune beneath the swampy swales, and also underlie the Great Dune. Medium- to coarse-grained sand with some beds of fine sand, gravelly sand, silty sand, sandy silt, and shelly sand make up the deposits. Above the water table these materials are generally shades of yellow and orange, indicating oxidizing geochemical conditions. Below the water table, colors range from shades of yellow and orange to gray, indicating a more reducing environment. Spit deposits range in thickness from about 12 to about 18 ft.

Gamma logs show that spit deposits emit relatively low amounts of radiation, which is consistent with the quartzose sand composition. EM logs of wet spit deposits have relatively low conductance readings.

*Swamp and marsh deposits*

Swamp/marsh deposits were encountered in two distinct settings. Hand auger borings and field observations revealed freshwater swamp deposits at the land surface in the low-lying swales located south of the Great Dune (Figs. 6 and 7) in an area that was mapped as spit deposits by Ramsey (2003). Swamp deposits differ from sandy spit deposits in that they are rich in organic material that contains recognizable leaves from trees, shrubs, and grasses. Swamp/marsh deposits were also encountered in three boreholes (Ni45-35, -37, and -46, Appendix A2) that penetrated through the dune deposits. Ni45-35 contained peat (sample 104972, Beta 266551) with an age of 720 to 920 years before present at a depth of 35 ft below land surface (bls) (-7 ft NAVD88). Because these three samples were collected beneath the Great Dune, the deposits must be older than both the Great Dune and the surficial swamp. Consistent with the older age, the plant remains in these boreholes are much more decomposed than those in the freshwater swamps. As a result of this decomposition, we cannot identify the plant types and definitively state whether the organic-rich beds found at depth in Ni45-35, Ni45-37, and Ni45-46 are freshwater swamp or marsh deposits, or saltwater marsh deposits. Chadwick (2000) concluded that the swamp and marsh materials were deposited in freshwater and saltwater environments that were short lateral and vertical distances from each other and the adjacent spit deposits.

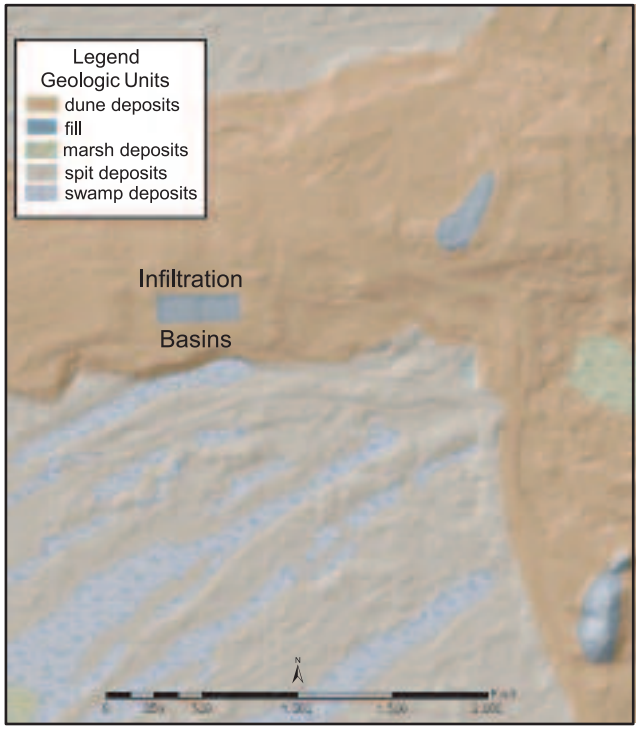


**Figure 6.** Surficial geologic map of CHSP study site. Geologic map of Ramsey (2003) modified from interpretation of field observations and LIDAR data. Shaded relief map created from LIDAR data.

The swamp/marsh deposits are very heterogeneous. These materials range from silty, peaty sands to sandy, silty, peats with scattered logs, partially carbonized wood fragments, possible charcoal, and pebbles. Organic matter ranges from relatively fresh, whole leaves and woody material at the surface to organic silt and small carbonized fragments at depths greater than 1 ft. These deposits emit gas bubbles with strong hydrogen sulfide odors when disturbed. Swamp/marsh deposits occur as discontinuous beds ranging in thickness from a few tenths of a foot to about 5 ft. The materials range in color from moderate to dark shades of brown and gray. The high organic content, brown and gray colors, and presence of gas indicate a strongly reducing environment. Gamma logs show that the swamp/marsh deposits emit higher amounts of radiation than the sandier dune and spit deposits, which is consistent with the organic-rich composition. EM logs show that swamp/ marsh deposits typically exhibit conductance readings that are greater than sandy, wet dune and spit deposits.

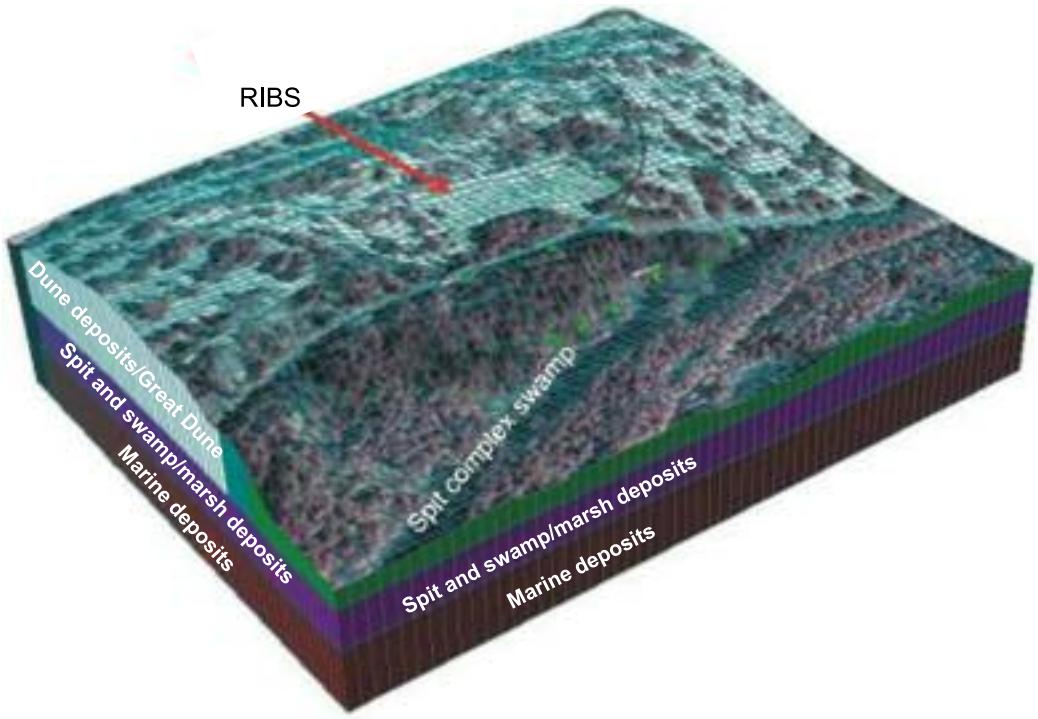


**Figure 7.** Block diagram showing surface and subsurface distribution of geologic units at CHSP study site. Base image is 2002 false color infrared aerial photograph draped on LIDAR-derived DEM.

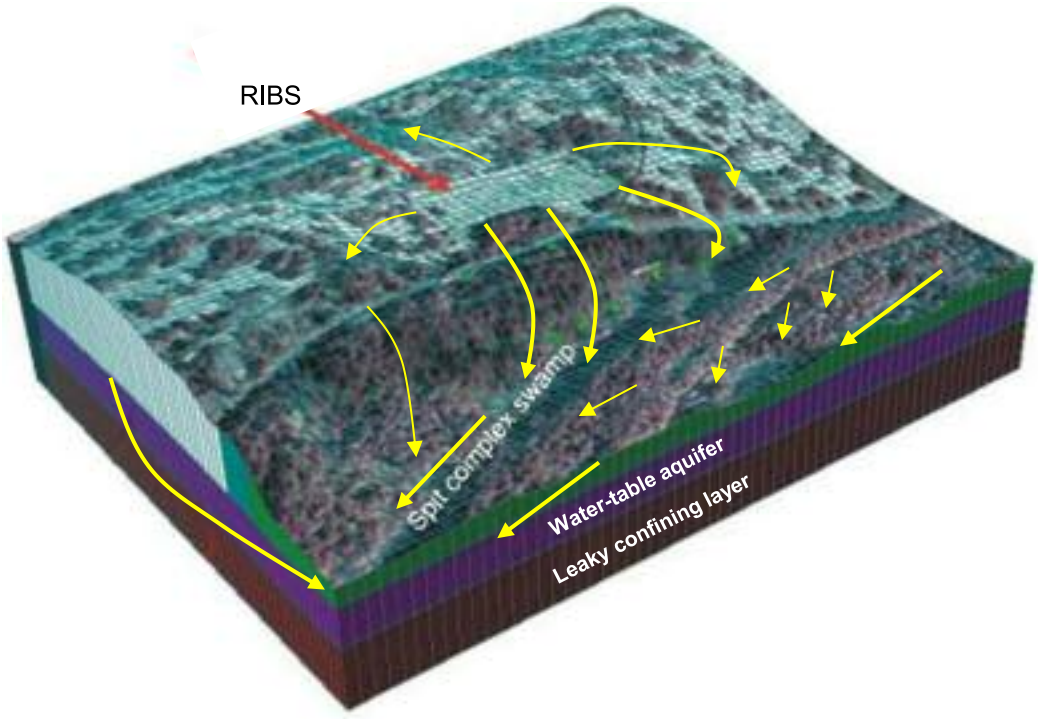


**Figure 8.** Block diagram showing conceptual hydrogeologic model. Groundwater flow paths and magnitudes are shown by yellow lines and arrows. Width of the flow lines indicates relative flow magnitude. Base image is 2002 false color infrared aerial photograph draped on LIDAR-derived DEM.

*Marine deposits*

Marine deposits are very heterogeneous, ranging from silty sands to sandy, clayey, silts. Colors vary from light yellow to dark brown and dark gray; the brown and gray shades are sometimes associated with hydrogen sulfide odors, indicating reducing conditions. Marine deposits, encountered in Ni45-33 and Ni45-35 (Appendix A2), interfinger with spit deposits. The entire thickness of this unit was not penetrated during this study. Gamma logs show that marine deposits emit higher amounts of radiation than dune and spit deposits, which is consistent with the silty and clayey composition. EM logs did not penetrate marine deposits.

*A note on geophysical logs*

Gamma logs run in the hollow stem auger and gamma logs run in the finished wells at the same locations show different patterns. Higher radiation values were observed in the finished wells in the intervals where bentonite pellets were used to seal the annular space between the casing and the borehole wall. EM logs run in the finished wells show higher conductance values in the same intervals. Much higher than ambient radiation values were observed when the gamma tool was placed in a bucket of bentonite pellets. This indicates that the bentonite pellets have significantly affected the response of the geophysical tool and masked the geophysical properties of the surrounding formation.

## Conceptual Hydrogeologic Model and Water-Table Configuration

Where saturated, dune and spit deposits function as a water table aquifer. Within the framework of DGS hydrostratigraphic nomenclature, this would be known as the Columbia aquifer. Much less permeable swamp/marsh and fine-grained marine deposits function as leaky confining beds. Existing data are not sufficient to determine the locations and characteristics of hydraulic connections between the Columbia and underlying aquifers.

The conceptual hydrogeological model for the study area is illustrated in Figure 8. Groundwater flows from topographically high areas (e.g., Great Dune) to topographically low areas. Beneath the highest portion of the Great Dune the water table is nearly 45 ft bls. South of the Great Dune within the proto-Cape Henlopen spit complex, the water table intersects and sometimes exceeds the land surface (Chadwick, 2000), creating a swampy area that will be referred to as the Spit Complex Swamp (SCS). The emergent water table similarly creates swampy areas in some of the deeper depressions within the area of the Great Dune to the east of the infiltration basins.

Discharge of effluent into the infiltration basins creates a water-table mound under the basins. The position and height of the mound change with time, to largely reflect changes in the rate and location of effluent discharge (Figs. 9-11). The steepest hydraulic gradient is directed toward the SCS.

Within the SCS, the land surface slopes westward toward the Lewes and Rehoboth Canal. The 1:24,000-scale USGS topographic map (Fig. 12) depicts streams as blue lines extending eastward from the canal into some portions of the SCS. However, because of the hummocky topography and dense vegetation, we were unable to identify a stream extending from the canal eastward to the area of the SCS just south of the infiltration basins. Rather, when the water-table elevation was high (e.g., spring 2009), we observed standing water in many poorly drained depressions. During drier periods, when the water table was low (e.g., summer and autumn 2008), the undrained depressions contained no standing water. As a result, we consider these features not to be streams but to be ephemeral groundwater-fed ponds.

Within the SCS, groundwater elevations were not measured so the water-table configuration and groundwater flow paths are conceptual. Given the westward slope of the land surface toward the canal and the water-table elevations observed in wells Ni45-38 through Ni45-42, we expect that flow within the SCS is also generally to the west. A secondary trend of directed flow to the northwest and southeast associated with higher water-table elevations under the low ridges is likely. Water quality data (Andres et al., 2015) do not indicate that groundwater originating from RIBS effluent is discharging into the ephemeral ponds described above.

Lesser gradients are directed from the infiltration basins towards the north, east, and west, although our understanding of water-table configuration and flow directions is limited because there are few monitoring wells in these areas. Water-table elevations from December 2008 (Fig. 10) indicate complex flow patterns east of the infiltration basins in areas of complex topography. This complex topography includes several deep, closed depressions that sometimes contain standing water. The combination of standing water and limited groundwater-level data indicate that the deep closed depressions are the sites of focused discharge.

## Hydraulic Testing Results

Hydraulic conductivity (K) values determined from slug tests range over one order of magnitude and are generally similar to the results of pumping tests reported by Leis (1974) (Table 1). Evaluation of K data (Appendix C) indicates that the interaction between well construction and lithology affects K observations. Slug test data from wells with 15-ft long screens that span the water table and are open to dune, spit, and swamp/marsh deposits are noisy, indicating problems with non-instantaneous displacement (Butler, 1998). Butler (1998) suggests that this may lead to the overestimation of K by at least 20 percent. Wells located in the SCS that are open to both freshwater swamp and spit deposits and were constructed with 2 to 3 ft of screen have K values four to five times lower than those in wells with 15 ft of screen. Test data from these wells is also less noisy than from the wells with 15 ft of screen. A third group of wells constructed by the U.S. Army Corps of Engineers with longer screens (>5 ft) that are open to dune and possibly spit deposits, have less than 5 ft of standing water, and have K values intermediate between the long screen wells and wells in the swamp and spit deposits. Though no wells were constructed to provide an estimate of the saturated K of an individual unit, the data indicate that the well-sorted and coarse-grained dune deposits tend to be more permeable than

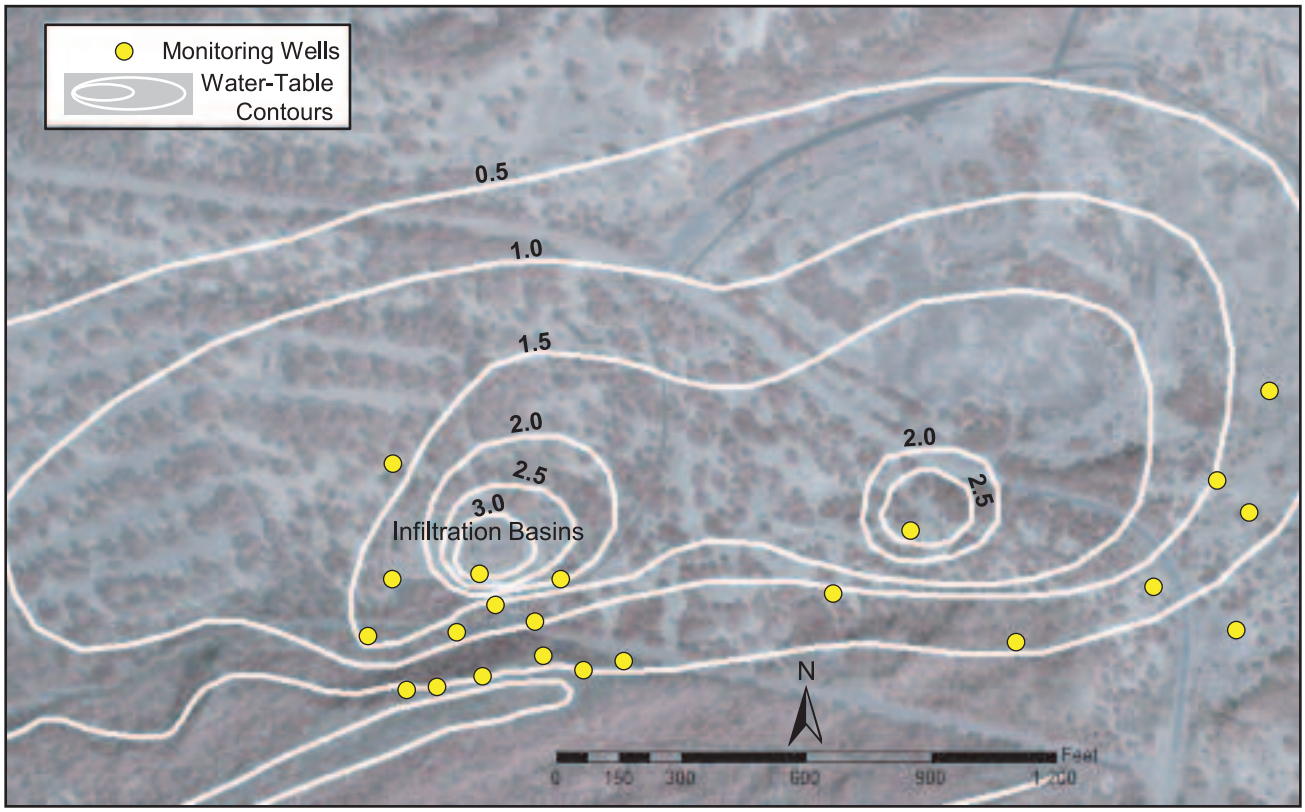


**Figure 9.** Water-table contour map for August 2008. Elevations are in feet, NAVD 1988.

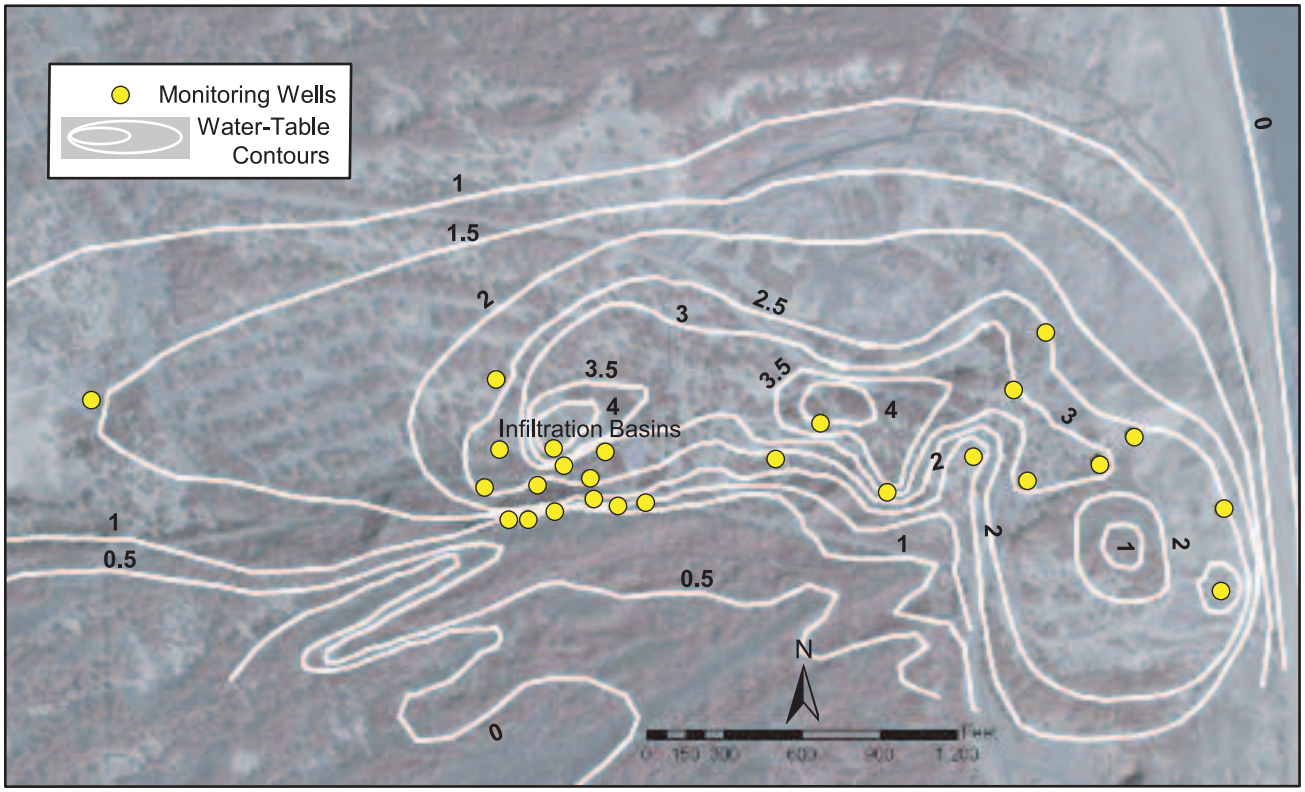


**Figure 10.** Water-table contour map for December 2008. Elevations are in feet, NAVD 1988.

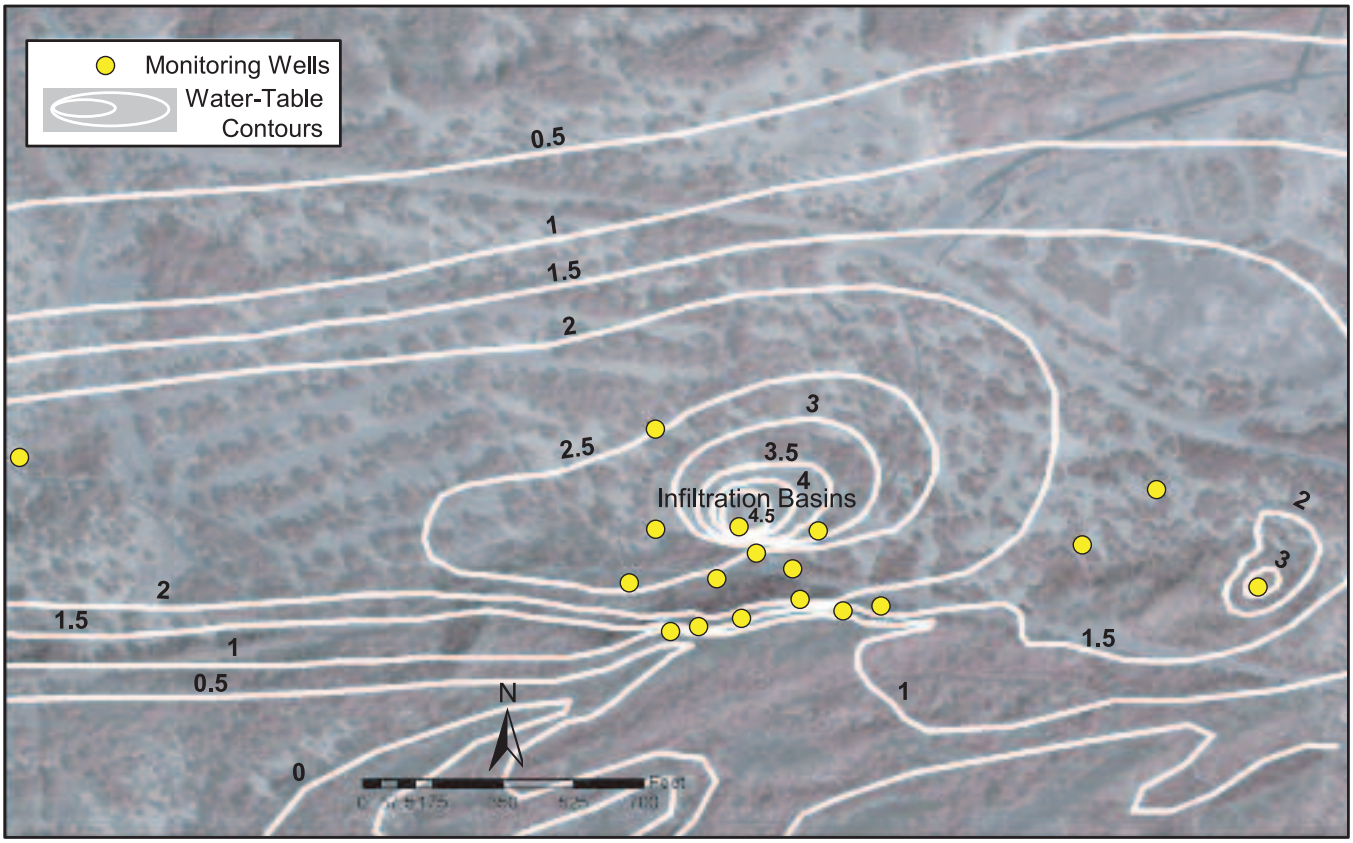


**Figure 11.** Water-table contour map for April 2009. Elevations are in feet, NAVD 1988.

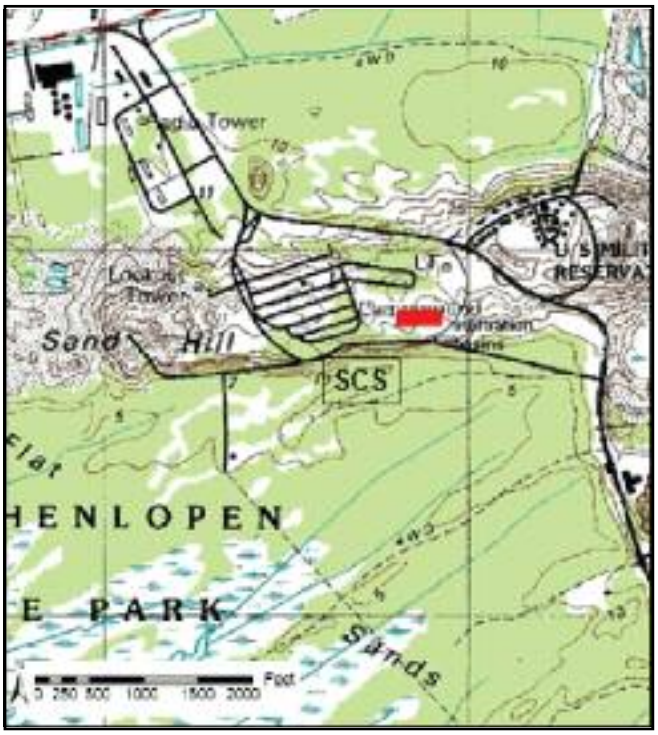


**Figure 12.** Reproduction of 1992 digital raster graphic topographic map. Red rectangle is the location of the infiltration basins.

the more heterogeneous and much finer grained freshwater swamp deposits. The results of a multi-well aquifer test reported by Leis (1974) are from wells with long (>15 ft) screens that are open to spit and shoreline deposits. The mean K value (94 ft/d) indicates that the K of spit deposits is only slightly less than those of dune sands (Leis, 1974).

The K values of the dune and spit deposits are similar to those reported for the clean sands of the Beaverdam, Bethany, and Cat Hill Formations (Andres, 2004; Andres and Klingbeil, 2006; DGS internal database). K values from the wells with 2- to 3-ft screens that are open to swamp/marsh deposits are greater than K values from swamp deposits of the Cypress Swamp Formation (mean K 7.7 ft/d, n=13; Andres and Howard, 2002, Table 2). However, considering that the wells tested in this study are open to both swamp/marsh deposits and more permeable spit deposits, the K values of the swamp/marsh deposits at Cape Henlopen are likely to be similar to those observed at the Cypress Swamp.

Infiltration rates (Table 2) resulting from double-ring infiltration tests (ASTM D3385) and conducted on both surficial and shallow (< 2 ft bls) subsurface materials, indicate that the materials in the basins should be classified as excessively well drained. Infiltration tests reveal higher infiltration rates in non-vegetated areas than in vegetated areas, consistent with greater proportions of organic matter in the vegetated areas. Subsurface moisture-content measurements made with the downhole TDR instrument showed that saturated or nearly saturated conditions (saturation >80 percent of porosity) were present to depths of 2.5 ft below surface prior to and during the test period indicating that the results represent the

**Table 1.** Results of hydraulic tests. Hydraulic conductivities in ft/d determined from slug tests. Group A includes wells with 15-ft screens, Group B includes wells with 2- to 3- ft screens, Group C includes wells installed by the US Army Corp of Engineers that have less than 10 ft of saturated material adjacent to the well screens. On the basis of a multi-well aquifer pumping test, Leis (1974) reports a mean K of 94 ft/d.

| | Group A | Group B | Group C |
|---|---|---|---|
| Minimum | 103 | 6.2 | 22 |
| Mean | 140 | 25 | 49 |
| Maximum | 179 | 49 | 70 |
| Standard Deviation | 26 | 19 | 20 |
| Count | 8 | 5 | 4 |

**Table 2.** Results of double-ring infiltration tests. Values are in feet per day. Data reported by Rufft (2009).

| DGSID | Date | K (ft/d) |
|---|---|---|
| Ni45-70 | 07/01/2009 | 64 |
| Ni45-73 | 07/09/2009 | 220 |
| Ni45-74 | 06/23/2009 | 92 |
| Ni45-76 | 07/30/2009 | 80 |
| Ni45-77 | 07/01/2009 | 160 |

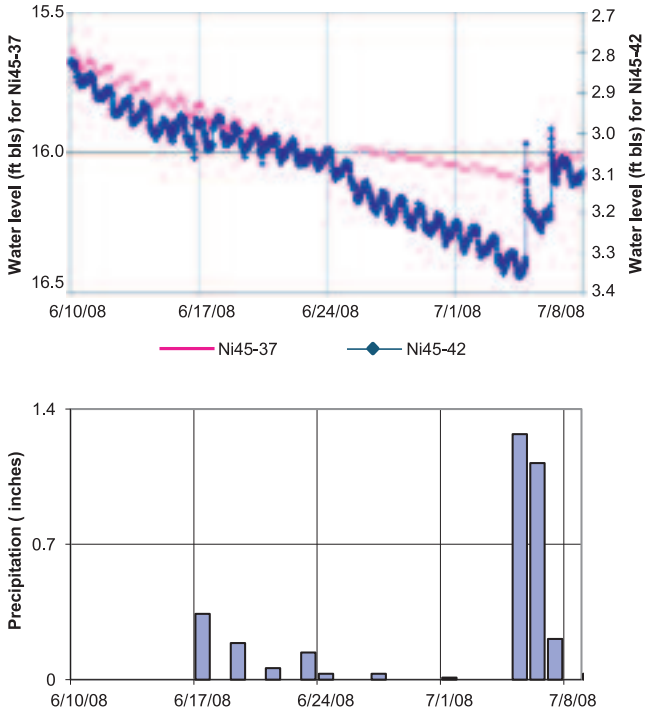


**Figure 13.** Example of hydrographs showing response to storm events. Precipitation measured at Lewes, DE. Note that water levels in well in swamp (Ni45-42) exhibit larger, more rapid response to storms between July 1 and July 8 than those in nearby well Ni45-37. See Figure 2 for well locations.

hydraulic properties of this interval. Given the overlapping K ranges of the single-well and double ring tests, it is very likely that the double ring test results reflect a combination of horizontal and vertical K rather than just vertical K.

### Water-Table and Water-Level Fluctuations

Groundwater levels in an unconfined aquifer in a coastal area are expected to change in response to changes in climate (e.g., precipitation and evaporation), transpiration by plants, tidal levels, pumping from wells, and the discharge of water to the water table. Our records and interviews with CHSP personnel indicate that there are no wells that are actively being pumped in the park.

Groundwater levels appear to vary according to proximity to the SCS. Wells in and near the SCS are influenced by short term climatic variations (Appendix D, Fig. 13). The SCS is frequently inundated after rainfall; for example, water levels measured in well Ni45-42 in the SCS, respond to individual storm events within hours (Fig. 13). Water levels in wells at higher elevations on the dune show progressively less of a response to storm events with increasing distance from the SCS. For example, water levels in Ni45-37 (Fig. 13) respond to storms in the same time frame as Ni45-42, but water levels in wells located farther from the SCS (e.g., Ni45-35, Fig. 14; Ni45-43, Ni45-44, Appendix D) do not appear to respond to storms. The lack of response to precipitation is likely due to the greater depth to water at these locations. We note that the one-day pattern observed in these hydrographs is related to effluent disposal (see below).

A tidal influence is not seen in the groundwater records. Groundwater-level records exhibit fluctuations with a period of roughly one day (Figs. 13 and 14) throughout the year. This pattern is in contrast to the tidal records from Breakwater Harbor (http://tidesandcurrents.noaa.gov/data_menu.shtml?stn=8557380%20Lewes,%20DE&type=Tide%20Data) and Rehoboth Bay (USGS Station 01484670), which have a semi-diurnal period.

Groundwater levels vary with proximity to the infiltration beds. Data loggers installed in wells located near the infiltration basins (Ni45-43, Fig. 14; Ni45-44, and 46, Appendix D) reveal a recurring pattern of water level height on an 8-day cycle. The patterns of peaks from an individual well are not in phase with patterns from the other wells, indicating that the patterns reflect the switch of effluent discharge between the eight beds. The data-logger-recorded water levels in all wells show a 1-day period that is thought to reflect the daily patterns of visitors and water use in the park (Appendix D). It is not clear if water-level records show increases associated with the increased discharge that occurs on weekends in response to the greater numbers of park visitors.

Given the dense vegetation and shallow water table in the SCS, we expected that the uptake of water by plants would be significant. Water-level records from Ni45-42 (Fig. 13) indicate that the fluctuations caused by effluent disposal mask the fluctuations due to transpiration. Transpiration measurement experiments were not conducted; however, summertime groundwater elevations in the swamp were at times below 0 ft NAVD88 (Appendix D). Because

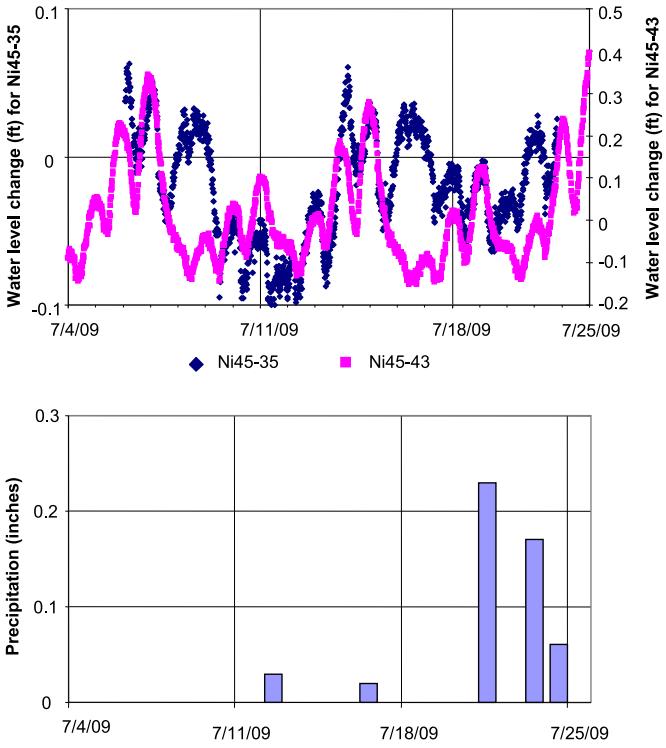


**Figure 14.** Examples of hydrographs showing effects of effluent discharge. Precipitation measured at Lewes, DE. Water levels have been processed using method illustrated in Figure 3 to enhance comparison of timing and magnitude of changes.

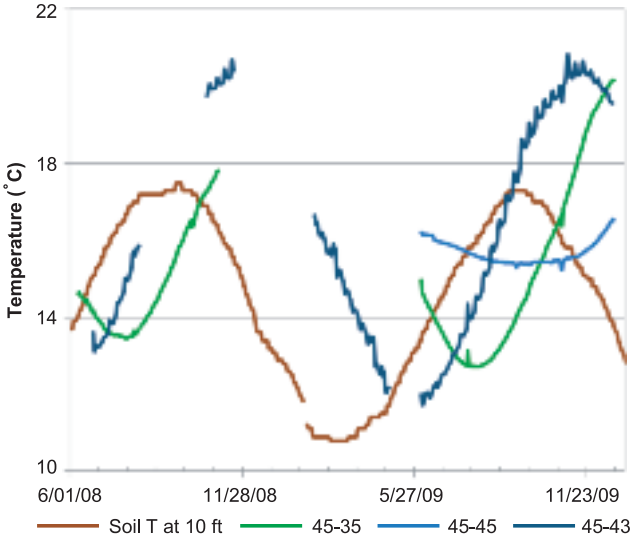


**Figure 15.** Soil temperature at 10 ft bls and groundwater temperatures in wells Ni45-35, 43, and 46. Soil temperature data provided by John Wehmiller of the University of Delaware Department of Geological Sciences (personnel communication). Measurement site located approximately 2500 ft west of infiltration beds at E491635, N4291684, altitude 22.8 ft. Coordinates in UTM18-83 in meters, altitude in ft NAVD88.

there is a lack of tidal influence and no pumping wells in the park, water elevations in the SCS less than this value can only be caused by transpiration.

### Water Temperature and Water-Level Fluctuations

Groundwater and soil temperatures recorded by data loggers and effluent temperature measurements provide additional information on the impacts of effluent disposal on the aquifer (Appendix D). Five effluent temperature measurements ranged from a low of 11.6°C, measured in April 2009, to a high of 22.3°C measured during July 2009. Groundwater temperatures greater than 20°C were observed in wells located under (Ni45-43) or immediately adjacent to the infiltration beds (Ni45-44, Ni45-46), and in Ni45-35, located about 80 ft downflow of the infiltration beds (Fig. 15, Appendix D). Mean groundwater temperatures in Ni45-43, 44, and 46 also showed daily summertime increases, indicating the discharge of warm effluent. The 20°C value is significant as greater ground-water temperatures have never been observed in Delaware in shallow (<30 ft deep) water-table wells having more than five years of continuous records (unpublished data from DGS database).

Of note is the relatively small variation of temperature in Ni45-33 (Appendix D), located north of the infiltration beds. Although water levels show the daily pressure signal due to wastewater discharge, the lack of a strong temperature signal indicates that not much flow is directed from the infiltration beds towards the north. Further, the relatively small magnitude of the annual groundwater temperature range in Ni45-33, compared to soil temperatures, indicates that the greater depth to groundwater in this well buffers groundwater temperature compared to seasonal atmospheric temperature fluctuations.

The temporal pattern and magnitude of temperature fluctuations observed in soil temperature probes and in wells Ni45-35, 43, and 45 (Fig. 15) and Ni45-34, 36, 37, 44 and 46, (Appendix D) reveal the movement of warmer effluent from the area under the infiltration beds toward the SCS. The maximum groundwater temperatures, which are several degrees higher than the soil temperatures, occur in the wells nearest the infiltration beds (listed in order of increasing distance from the infiltration beds, Ni45-43, 44, 46, and 35). Groundwater temperatures should not exceed soil temperatures unless there is an external source of heat, such as warm wastewater.

The groundwater temperature signal also varies with distance from the infiltration beds. Temperatures respond first in Ni45-43, closest to the infiltration beds; next in Ni45-35, approximately 90 ft from Ni45-43 and 80 ft from the nearest infiltration basin; and last in Ni45-45, approximately 160 ft from Ni45-43 and about 150 ft from the nearest infiltration bed (Fig. 15). The offset in the timing of minimum temperatures between wells indicate apparent transport times of about 45-55 days between Ni45-43 and Ni45-35, and 90-100 days between Ni45-43 and Ni45-45, signifying apparent flow velocities between 1.6 and 2 ft/d.

Groundwater temperatures in wells Ni45-34, 36, and 37 (Appendix D) located downgradient and slightly east and west of the infiltration basins are elevated above soil temperatures though maximum temperatures are estimated to not reach 20°C. Though temperatures are clearly affected by effluent discharge, daily temperature fluctuations are not observed in these wells as they are in wells Ni45-35 and 43 (Fig. 15) and Ni45-44 and 46 suggesting the temperature signal is masked by a combination of attenuation by the aquifer

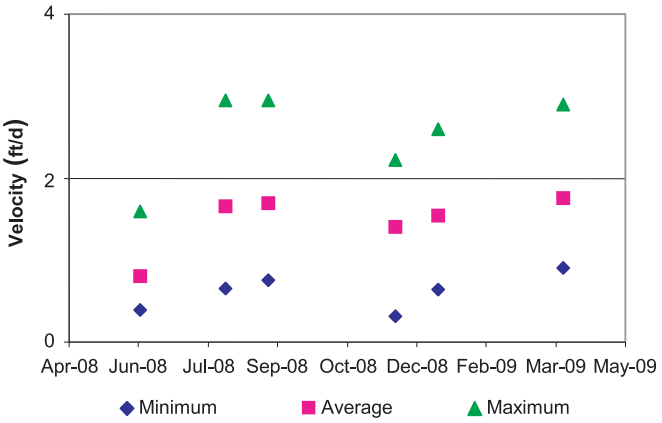


**Figure 16.** Comparison of monthly flow velocities as determined by simple two-dimensional particle tracking.

matrix and by mixing with groundwaters originating outside of the infiltration basins and not affected by effluent discharge.

### Flow Magnitude and Velocity

The gridded water-table configuration data was analyzed using simple Darcy's Law calculations and particle tracking. In this steady state model, the average K from slug tests and measured groundwater levels were used to define the K and pressure inputs. Key assumptions in this model included two-dimensional flow and a homogeneous, isotropic aquifer. As with nearly all models, there are differences between model assumptions and field conditions. At this site, there is likely to be a three-dimensional component to groundwater flow; hydraulic testing indicates that K varies by a factor of 10 to 15. While we understand that the model cannot precisely reproduce field conditions as formulated, it does provide useful information for computing and interpreting flow directions and velocities.

Model results indicate that inter-monthly variations in flow velocity are on the order of 2 or less (Fig. 16). The lack of greater flow velocity during the wetter months (i.e., greater inter-monthly variation) when the water-table elevation is higher indicates that wastewater discharge smoothes climate-induced variability. Intra-monthly ratios between maximum and minimum velocities are on the order of 3 to 6.5, with the maximum velocities associated with particle tracks directed from the southern half of the infiltration basins toward the SCS (Fig. 17). Given the positive correlation between flow velocity and water flux, particle tracks indicate preferential flow towards the SCS.

The results of a 180-day particle tracking simulation using average water-table elevations (Fig. 17) show that many of the flow paths originating along the southern side of the infiltration basins reach the SCS within 180 days. We predict that any vertical groundwater flow would have proportionally more impact on the lengths and orientation of the shorter flow paths directed toward the north, east, and west than on the flow paths directed southward toward the SCS. That is, flow paths on Figure 17 directed toward the north, east, and west will be diverted downwards and southward. An enhanced vertical component would also partially explain the spatial patterns of groundwater temperatures and daily temperature fluctuations. Figure 18 depicts these phenomena as a preferential flow zone and a mixing zone.

Particle tracking simulations are a first cut for assessing the potential effects of RIBS on ground and surface water. Because field data show that aquifer K and thickness are spatially heterogeneous, and because water-table gradients vary from month-to-month, the flows computed from homogeneous grids and long-period averaged water-table elevations have an unknown amount of uncertainty. The uncertainty in flow paths and flow magnitudes can be better quantified through the use of three-dimensional numerical models that incorporate spatially heterogeneous aquifer conditions and transient differences in flow.

## CONCLUSIONS

Our investigation of a rapid infiltration basin system (RIBS) at CHSP was used to develop a conceptual model of the hydrogeological framework in the vicinity of the infiltration basins and nearby discharge area. The water-table aquifer in geologically young (<1000 years) dune, spit, swamp, and marsh deposits is underlain by a leaky confining layer formed by marine deposits. Infiltration testing of dune deposits in the vadose zone indicates that these deposits are excessively well drained. Slug tests show that the water-table aquifer is moderately permeable.

Groundwater flow is driven by wastewater discharge, topographic, and climatic factors; there is no apparent tidal forcing. The effects of storms and wastewater discharge on the water-table aquifer are clearly seen in the water levels and temperatures measured by data logging instruments. These data show that wastewater discharge is the dominant forcing mechanism driving most flow from the infiltration beds toward the swampy discharge area located at sea level between 250 and 330 ft south of the infiltration beds. An unquantified, but minor amount of flow is directed from the infiltration beds towards the north.


**Figure 17.** Results of particle tracking for 180 day simulation under average flow conditions. Base map image is 2002 false color infrared aerial photograph with LIDAR-derived shaded relief DEM.

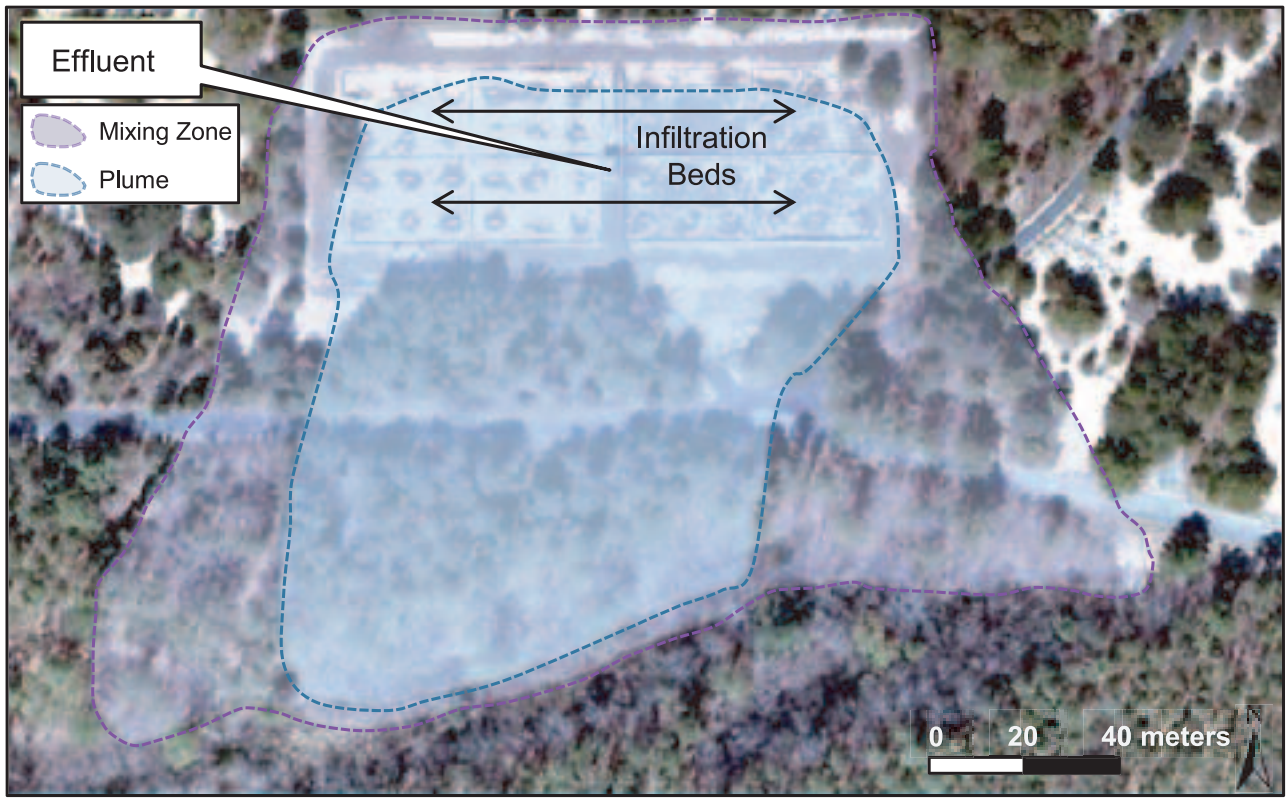


**Figure 18.** Illustration of preferential flow zone (plume) and mixing zone caused by disposal of treated wastewater.

## REFERENCES CITED


American Society for Testing and Materials (ASTM), 2003, Standard Test Method for Infiltration Rate of Soils in Field Using Double-Ring Infiltrometer, D3385-03.

Andres, A.S., 1991, Results of the Coastal Sussex County, Delaware Ground-Water Quality Survey: Delaware Geological Survey Report of Investigation No. 49, 28 p.

Andres, A. S., and Howard, C. S., 2002, Results of hydrogeologic studies of the Cypress Swamp Formation, Delaware: Delaware Geological Survey Report of Investigations No. 64, 18 p.

Andres, A. S., 2004, Ground-water recharge mapping in Kent and Sussex counties, Delaware: Delaware Geological Survey Report of Investigations No. 66, 20 p.

Andres, A. S., and Klingbeil, A. K., 2006, Thickness and transmissivity of the unconfined aquifer of eastern Sussex County, Delaware: Delaware Geological Survey Report of Investigations No. 70, 19 p., 1 pl.

Andres, A. S., Walther, E. F., Türkmen, M., He, C., Chirnside, A.E.M., and Ritter, W. F., 2015, Groundwater quality and monitoring of rapid infiltration basin systems, theory and field experiments at Cape Henlopen State Park, Delaware: Delaware Geological Survey Bulletin 21C, 46 p.

Ator, S. W., 2008, Natural and Human Influences on Water Quality in a Shallow Regional unconsolidated Aquifer, Northern Atlantic Coastal Plain, U.S. Geological Survey Scientific Investigations Report 2008-5190, 32 p.

Bear, J., 1979, Hydraulics of groundwater: New York, McGraw-Hill, 569 p.

Bouwer, H., 1989, The Bouwer and Rice slug test - an update: Ground Water, vol. 27, no. 3, pp. 304-309.

Butler, J. J., 1998, The design, performance, and analysis of slug tests: Boca Raton, Lewis Publishers, 252 p.

Chadwick, W. J., 2000, Paleographic and paleoenvironmental reconstruction of terrain associated with coastal prehistoric archaeological sites, Cape Henlopen, Delaware: University of Delaware, Ph.D. dissertation.

Debrewer, L. M., Ator, S. W., and Denver, J. M., 2005, Factors Affecting Spatial and Temporal Variability in Nutrient and Pesticide Concentrations in the Surficial Aquifer on the Delmarva Peninsula, U.S. Geological Survey Scientific Investigations Report 2005-5257, 56 p.

Denver, J.M., Ator, S.W., Debrewer, L.M., Ferrari, M.J., Barbaro, J.R., Hancock, T.C., Brayton, M.J., and Nardi, M.R., 2004, Water Quality in the Delmarva Peninsula, Delaware, Maryland, and Virginia, 1999–2001: U.S. Geological Survey Circular 1228, 27 p.

Guitierrez-Magness, A. L., and Raffensperger, J. P., 2003, Development, Calibration, and Analysis of a Hydrologic and Water-Quality Model of the Delaware Inland Bays Watershed, U.S. Geological Survey Water Resources Investigation Report 03-4124, 46 p.

Kramer, M. G., 1987, Delaware Geological Survey laboratory procedures manual: Delaware Geological Survey Special Publication 15.

Laurent, J. P., Ruelleb, P., Delageb, L., Abdelaziz, Z., Béchir, B. N., and Adjmic, T., 2005, Monitoring Soil Water Content Profiles with a Commercial TDR System Comparative Field Tests and Laboratory Calibration: Vadose Zone Journal, p. 1030-1036.

Leis, W. M., 1974, Artificial recharge in coastal Sussex County, Delaware: University of Delaware Water Resources Center, 100 p.

Miller, J.C., 1972, Nitrate Contamination of the Water-Table Aquifer in Delaware: Delaware Geological Survey Report of Investigations No. 20, 36 p.

Pellerito, V., Neimester, M.P., Wollf, E., and Andres, A.S., 2006, Results of the Domestic Well Water Quality Study: Delaware Geological Survey Open File Report No. 48, 50 p.

Ramsey, K. W., 2003, Geologic map of the Lewes and Cape Henlopen quadrangles, Delaware: Delaware Geological Survey Geologic Map No. 12, 1:24,000.

Ritter, W.F., and Chirnside, A.E.M., 1982, Ground water quality in selected areas of Kent and Sussex Counties, Delaware: Agriculture Experiment Station. University of Delaware.

Ritter, W.F., and Chirnside, A.E.M., 1984, Impact of Land Use on Ground-Water Quality in Southern Delaware: Ground Water, v. 22, p. 38-47.

Robertson, F.W., 1977, The Quality and Potential Problems of Ground Water In Coastal Sussex County, Delaware: University of Delaware Water Resources Center, 58 p.

Robinson, D. A., Jones, S. B., Wraith, J. M., Or, D., and Friedman, S. P., 2003, A Review of Advances in Dielectric and Electrical Conductivity Measurement in Soils Using Time Domain Reflectometry: Vadose Zone Journal, p. 444-475.

Rufft, J., 2009, Physcial characterization of rapid infiltration basin systems used for wastewater and stormwater disposal: Delaware Water Resources Center, University of Delaware, 20 p.

Schlumberger Water Systems, 2008, Aquifer Test Pro software, Waterloo, Ontario.

Türkmen, M., Walther, E. F., Andres, A. S., Chirnside, A. E., and Ritter, W. F., 2008, Evaluation of rapid infiltration basin systems (RIBS) for wastewater disposal: Phase I: Delaware Geological Survey unpublished contract report to DNREC, 41 p.

US Army Corps of Engineers, 1997, Site inspection report – former Fort Miles Military Reservation, Sussex County, Delaware: Baltimore, Maryland, US Army Corps of Engineers Engineering Division,

USDA Web Soil Survey, http://websoilsurvey.nrcs.usda.gov/app/WebSoilSurvey.aspx, accessed July 27, 2009.

**APPENDIX A1.** Construction information for wells used in this study.

| DGS Well Identifier | DNREC permit | Top of casing elevation (ft NAVD88) | Land surface elevation (ft NAVD88) | Depth to top of screen (ft bls) | Depth to bottom of screen (ft bls) | Map index number | NOTE |
|---|---|---|---|---|---|---|---|
| Ni44-16 | 109284 | 44.97 | 42.97 | 34.6 | 44.6 | 1 | USACE |
| Ni45-15 | 109275 | 21.87 | 19.87 | 13 | 23 | 2 | USACE |
| Ni45-16 | 109276 | 30.14 | 27.64 | 19 | 29 | 3 | USACE |
| Ni45-17 | 109277 | 23.87 | 21.87 | 14.5 | 24.5 | 4 | USACE |
| Ni45-18 | 109278 | 14.62 | 12.12 | 4 | 14 | 5 | USACE |
| Ni45-33 | 223154 | 46.52 | 44.32 | 45 | 60 | 6 | |
| Ni45-34 | 223155 | 30.52 | 28.92 | 30 | 45 | 7 | |
| Ni45-35 | 223156 | 32.13 | 29.43 | 30 | 45 | 8 | |
| Ni45-36 | 223157 | 28.07 | 25.77 | 25 | 40 | 9 | |
| Ni45-37 | 223158 | 17.1 | 14.9 | 19.5 | 34.5 | 10 | |
| Ni45-38 | 223159 | 3.96 | 1.36 | 1.4 | 3.9 | 11 | |
| Ni45-39 | 223160 | 6.78 | 5.46 | 2.1 | 4.6 | 12 | |
| Ni45-40 | 223161 | 3.83 | 3.05 | 2.5 | 5 | 13 | |
| Ni45-41 | 223162 | 7.37 | 5.67 | 3.1 | 5.6 | 14 | |
| Ni45-42 | 223163 | 3.97 | 1.47 | 0.5 | 2.5 | 15 | |
| Ni45-43 | 224318 | 37.18 | 37.18 | 30 | 45 | 16 | |
| Ni45-44 | 224319 | 37.82 | 35.82 | 30 | 45 | 17 | |
| Ni45-45 | 224320 | 30.49 | 28.49 | 25 | 40 | 18 | |
| Ni45-46 | 224324 | 34.5 | 32.5 | 30 | 45 | 19 | |
| Ni45-47 | 225308 | 3.51 | 1.51 | 33.4 | 33.7 | 16 | |
| Ni45-48 | 225309 | 3.51 | 1.51 | 36.9 | 37.2 | 16 | |
| Ni45-49 | 225310 | 3.51 | 1.51 | 40.4 | 40.7 | 16 | |
| Ni45-50 | 225311 | 3.51 | 1.51 | 43.9 | 44.2 | 16 | |
| Ni45-51 | 225312 | 3.51 | 1.51 | 47.4 | 47.7 | 16 | |
| Ni45-52 | 225313 | 3.51 | 1.51 | 50.9 | 51.2 | 16 | |
| Ni45-53 | 225314 | 3.51 | 1.51 | 54.4 | 54.7 | 16 | |
| Ni45-54 | 225335 | 30.49 | 30.49 | 26.4 | 26.7 | 18 | |
| Ni45-55 | 225336 | 30.49 | 30.49 | 29.9 | 30.2 | 18 | |
| Ni45-56 | 225337 | 30.49 | 30.49 | 33.4 | 33.7 | 18 | |
| Ni45-57 | 225338 | 30.49 | 30.49 | 36.9 | 37.2 | 18 | |
| Ni45-58 | 225339 | 30.49 | 30.49 | 40.4 | 40.7 | 18 | |
| Ni45-59 | 225340 | 30.49 | 30.49 | 43.9 | 44.2 | 18 | |
| Ni45-60 | 225341 | 30.49 | 30.49 | 47.4 | 47.7 | 18 | |
| Ni45-61 | 225315 | 5.97 | 3.97 | 28.8 | 29.1 | 8 | |
| Ni45-62 | 225316 | 5.97 | 3.97 | 31.8 | 32.1 | 8 | |
| Ni45-63 | 225317 | 5.97 | 3.97 | 35.8 | 36.1 | 8 | |

Note: USACE - US Army Corps of Engineers well
ft bls - feet below land surface.

**APPENDIX A1.** Construction information for wells used in this study (continued).

| DGS Well Identifier | DNREC permit | Top of casing elevation (ft NAVD88) | Land surface elevation (ft NAVD88) | Depth to top of screen (ft bls) | Depth to bottom of screen (ft bls) | Map index number | NOTE |
|---|---|---|---|---|---|---|---|
| Ni45-64 | 225318 | 5.97 | 3.97 | 40.3 | 40.6 | 8 | |
| Ni45-65 | 225319 | 5.97 | 3.97 | 44.8 | 45.1 | 8 | |
| Ni45-66 | 225320 | 5.97 | 3.97 | 49.3 | 49.6 | 8 | |
| Ni45-67 | 225321 | 5.97 | 3.97 | 51.8 | 52.1 | 8 | |
| Ni45-78 | 224321 | 1.9 | -0.1 | 1 | 1.3 | 15 | |
| Ni45-79 | Ni4579 | 33 | 31 | 2.5 | 2.8 | 15 | |
| Ni45-80 | Ni4580 | 33 | 31 | 4 | 4.3 | 15 | |
| Ni45-81 | Ni4581 | 33 | 31 | 5.5 | 5.8 | 15 | |
| Ni45-82 | Ni4582 | 33 | 31 | 7 | 7.3 | 15 | |
| Ni45-83 | Ni4583 | 33 | 31 | 8.5 | 8.8 | 15 | |
| Ni45-84 | Ni4584 | 33 | 31 | 10 | 10.3 | 15 | |
| Ni45-85 | | 11.57 | 10.5 | 10.1 | 15.1 | 20 | USACE |
| Ni45-86 | | 7.8 | 6.8 | 10.1 | 15.1 | 21 | USACE |
| Ni45-87 | | 9.28 | 6.3 | 10.1 | 15.1 | 22 | USACE |
| Ni45-88 | | 13.14 | 10.1 | 10.1 | 15.1 | 23 | USACE |
| Ni45-89 | | 24.55 | 22.5 | 20.1 | 30.1 | 24 | USACE |
| Ni45-90 | | 60.41 | 56.4 | 55.7 | 65.7 | 25 | USACE |
| Ni45-91 | | 32.58 | 31.5 | 24.5 | 34.5 | 26 | USACE |

Note: USACE - US Army Corps of Engineers well
ft bls - feet below land surface.

**APPENDIX A2.** Descriptive and geophysical logs for wells used in this study.

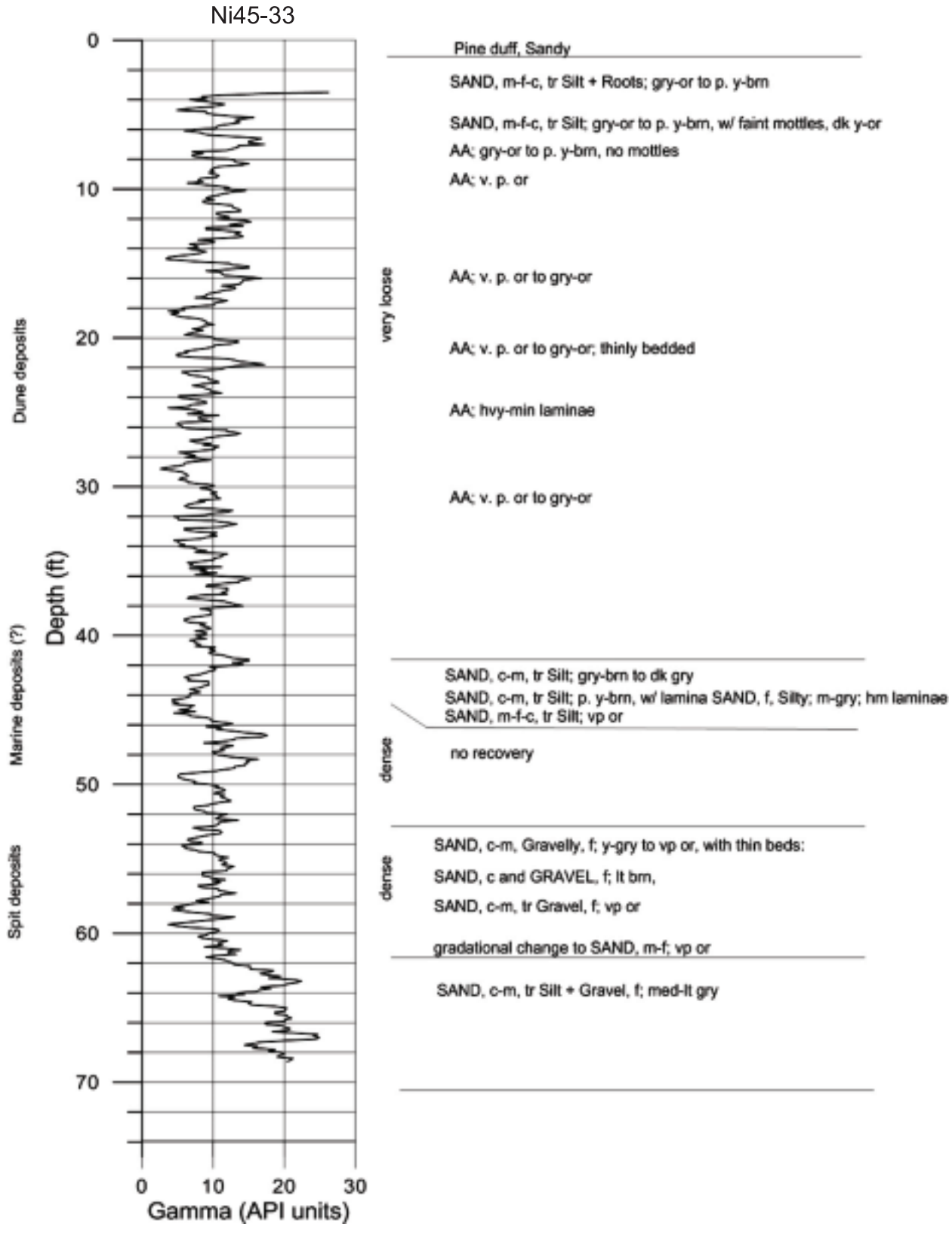

**APPENDIX A2.** Descriptive and geophysical logs for wells used in this study (continued).

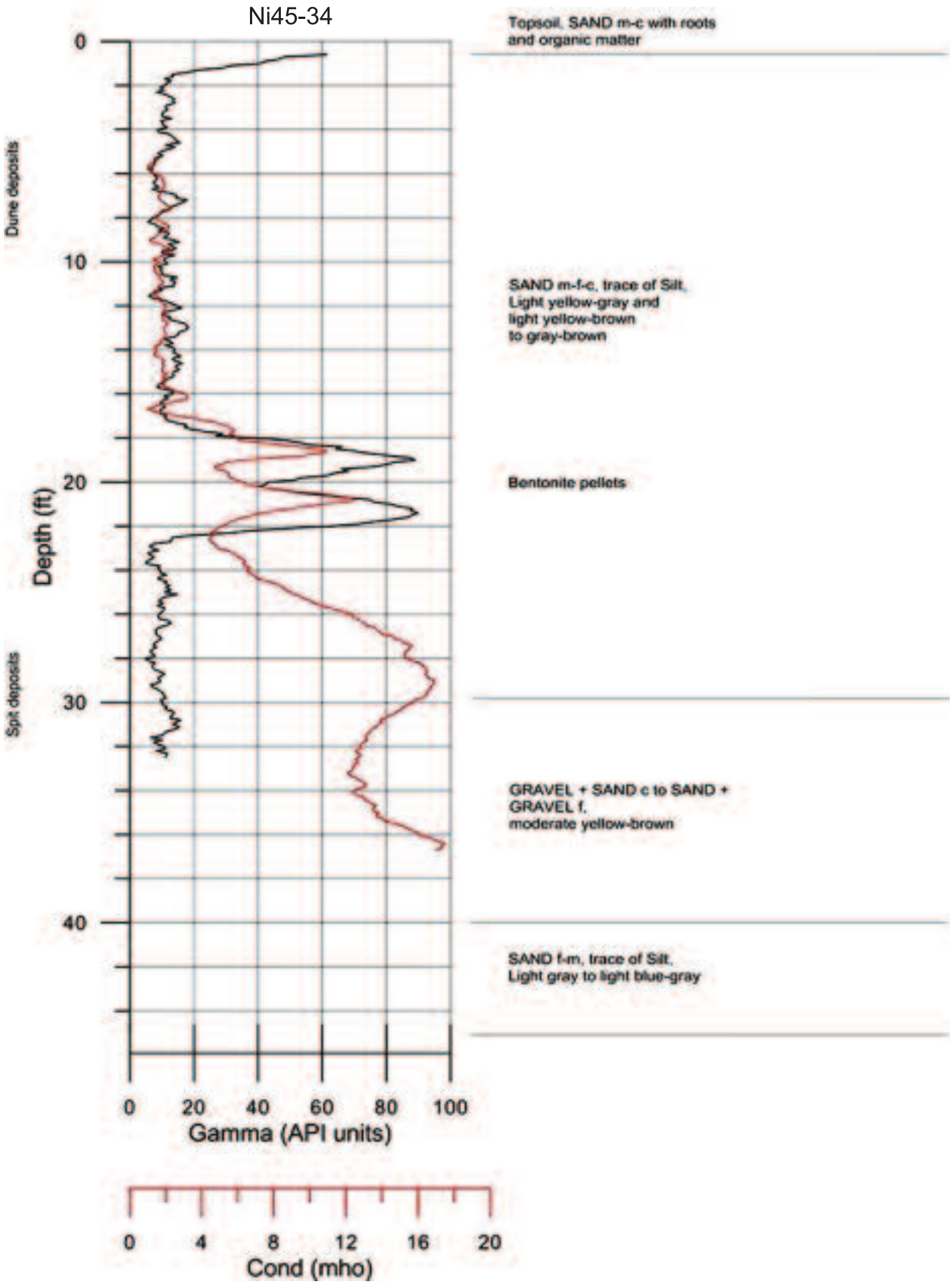

**APPENDIX A2.** Descriptive and geophysical logs for wells used in this study (continued).

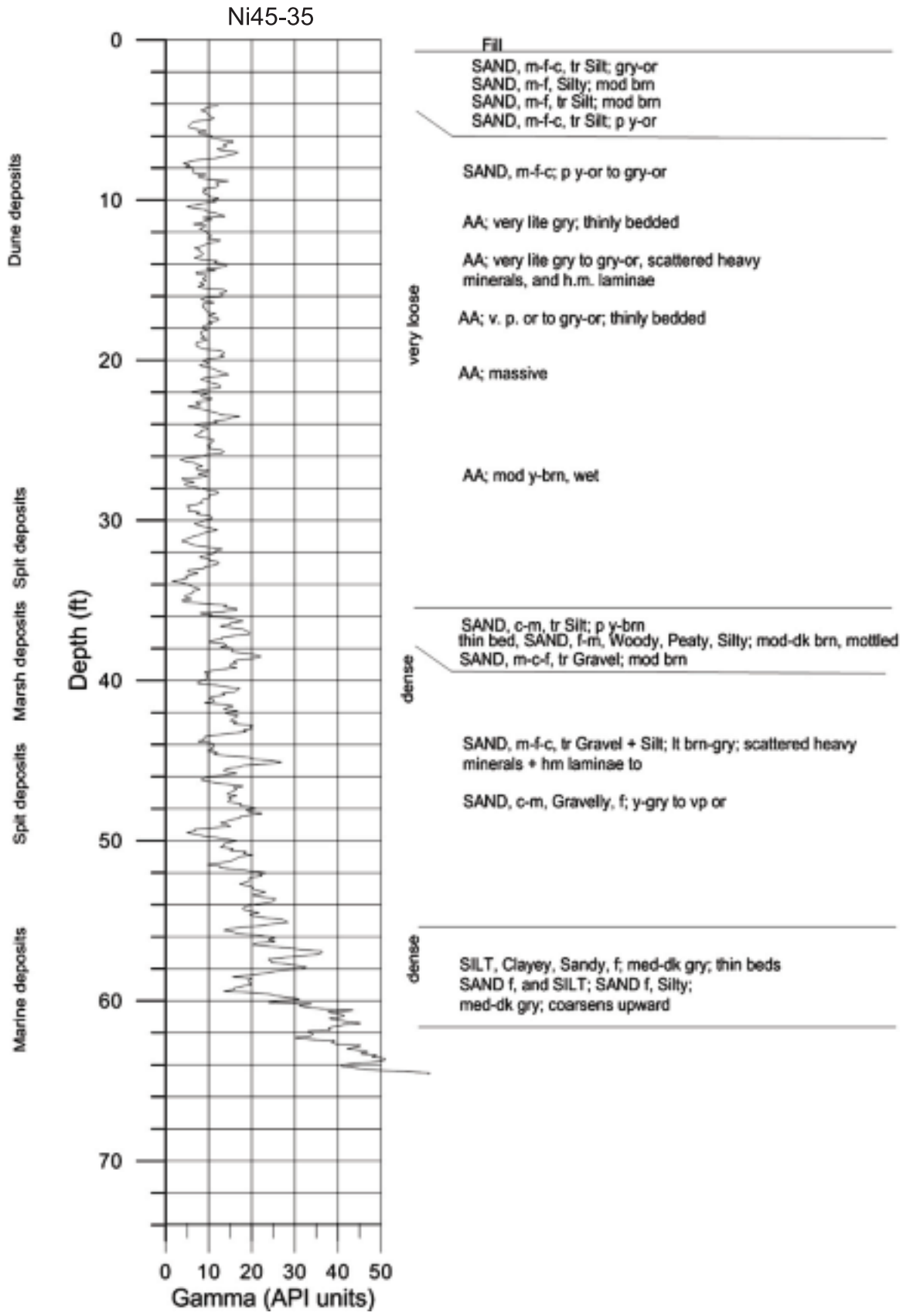

**APPENDIX A2.** Descriptive and geophysical logs for wells used in this study (continued).

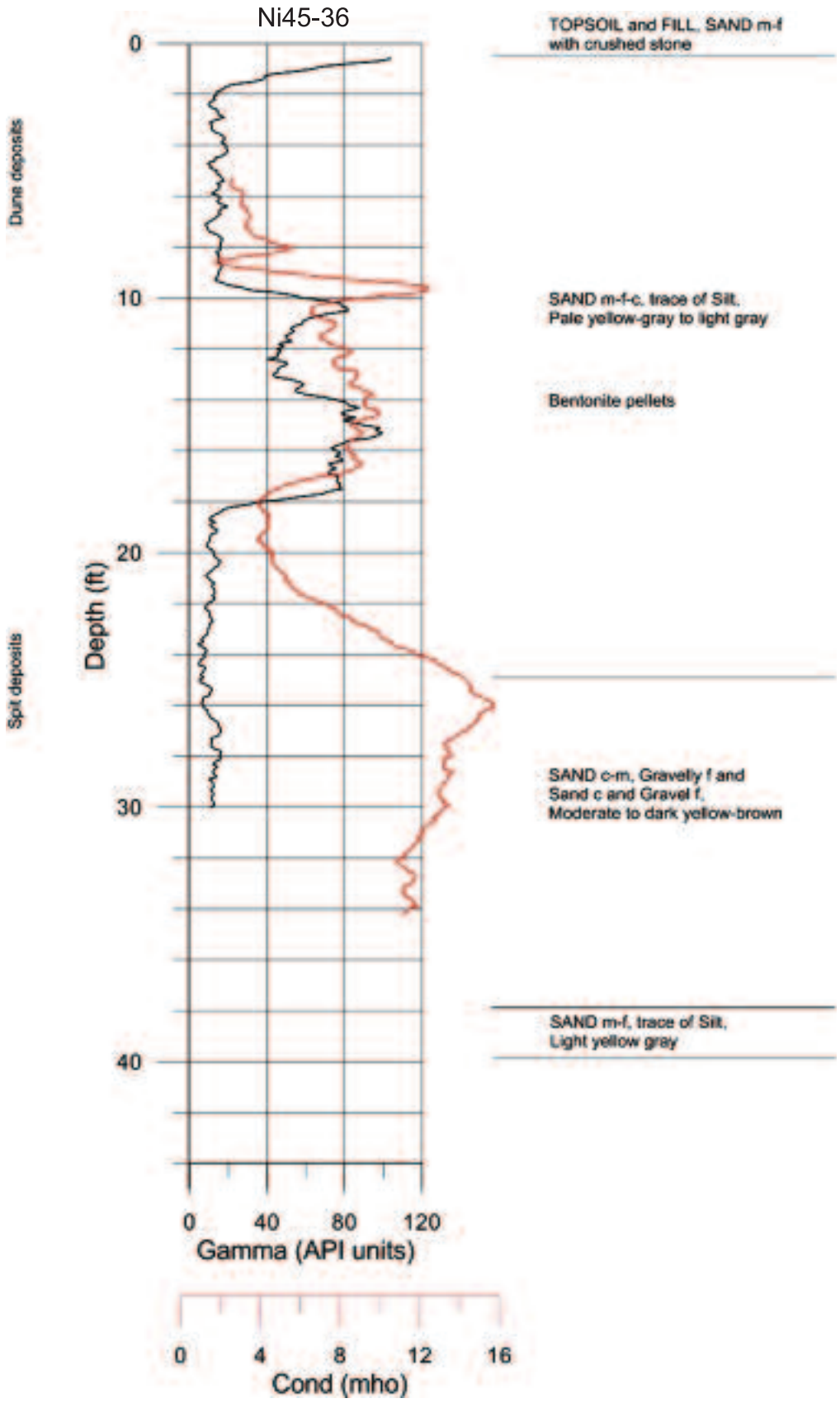

**APPENDIX A2.** Descriptive and geophysical logs for wells used in this study (continued).

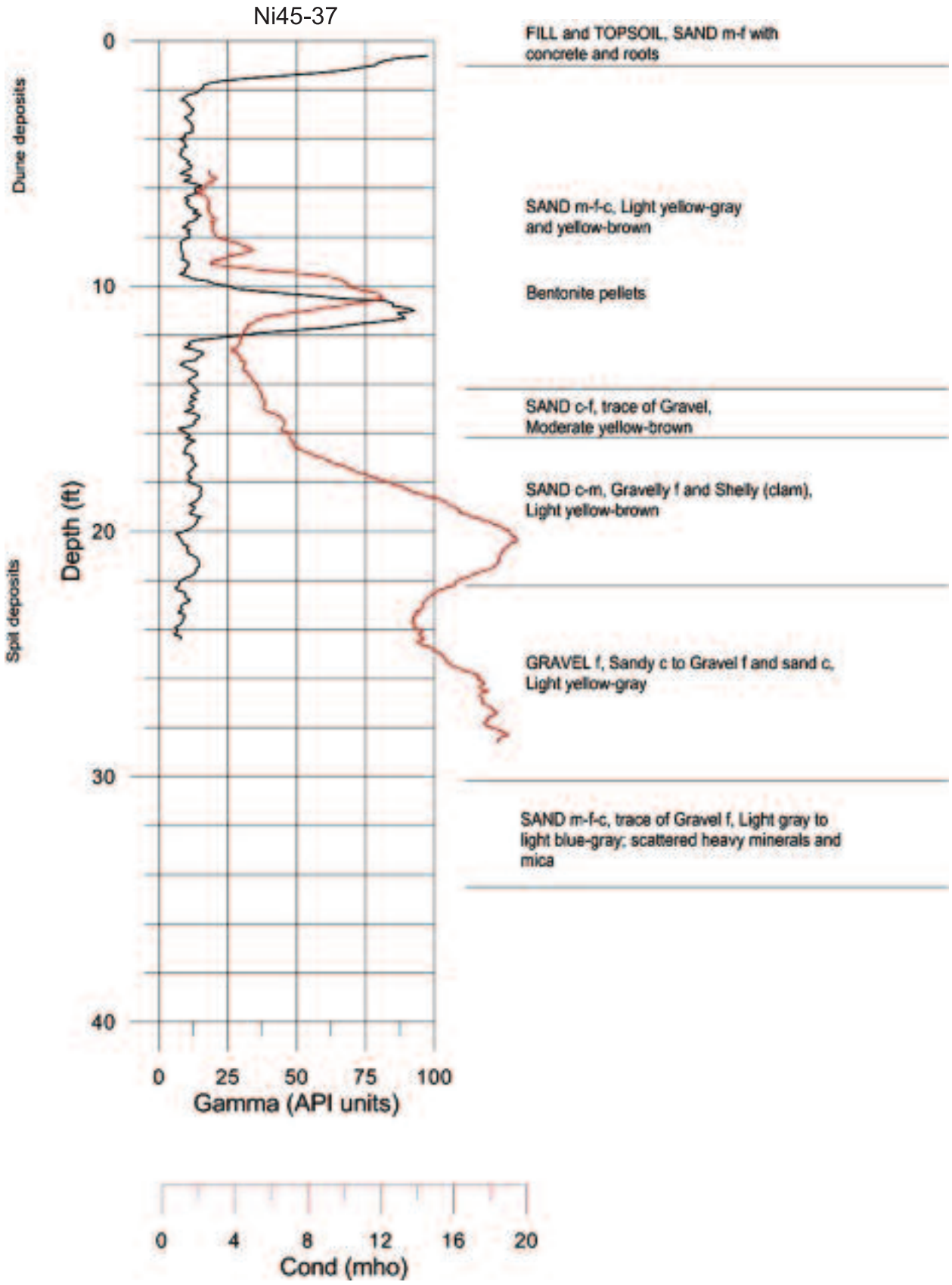

**APPENDIX A2.** Descriptive and geophysical logs for wells used in this study (continued).

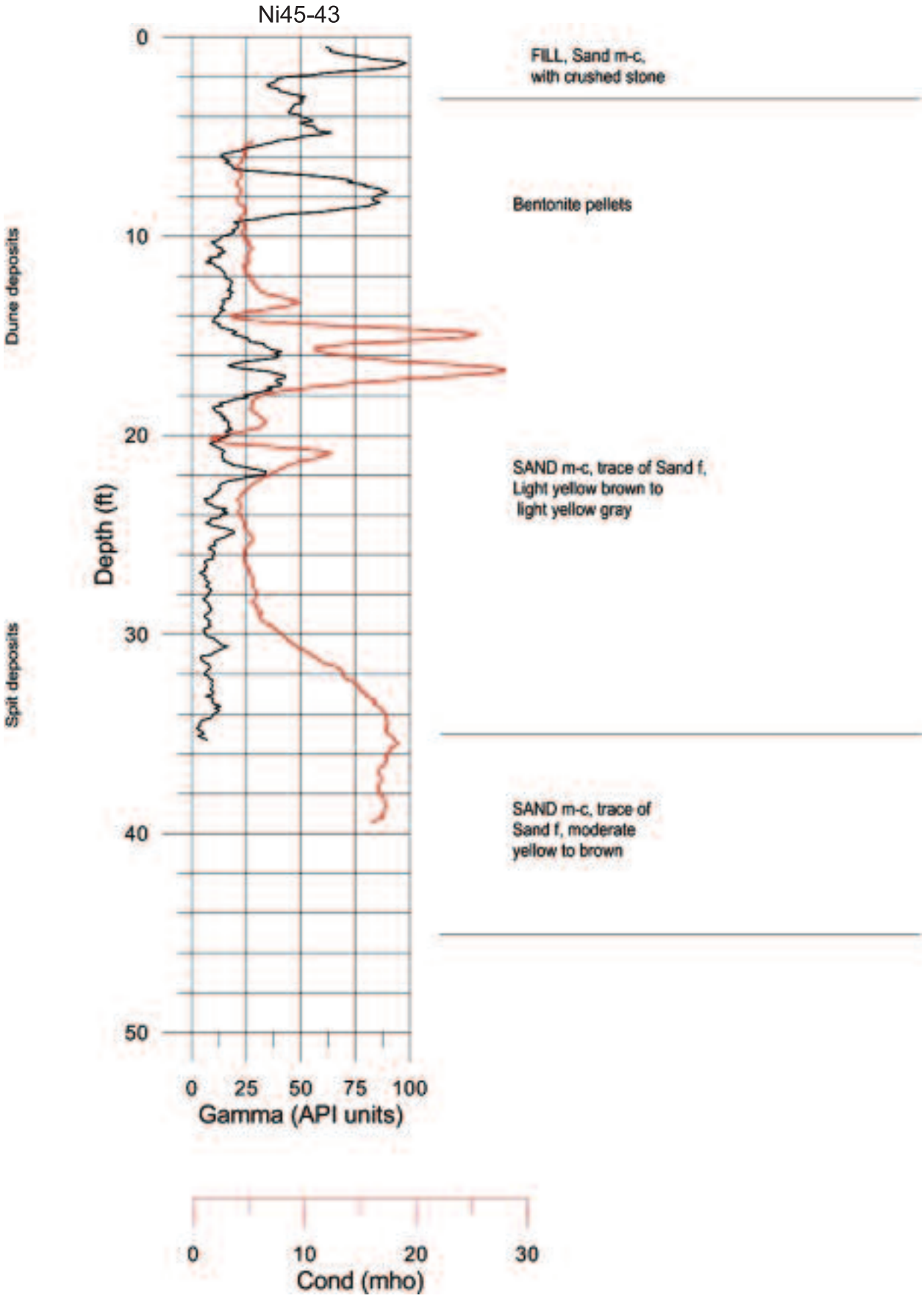

**APPENDIX A2.** Descriptive and geophysical logs for wells used in this study (continued).

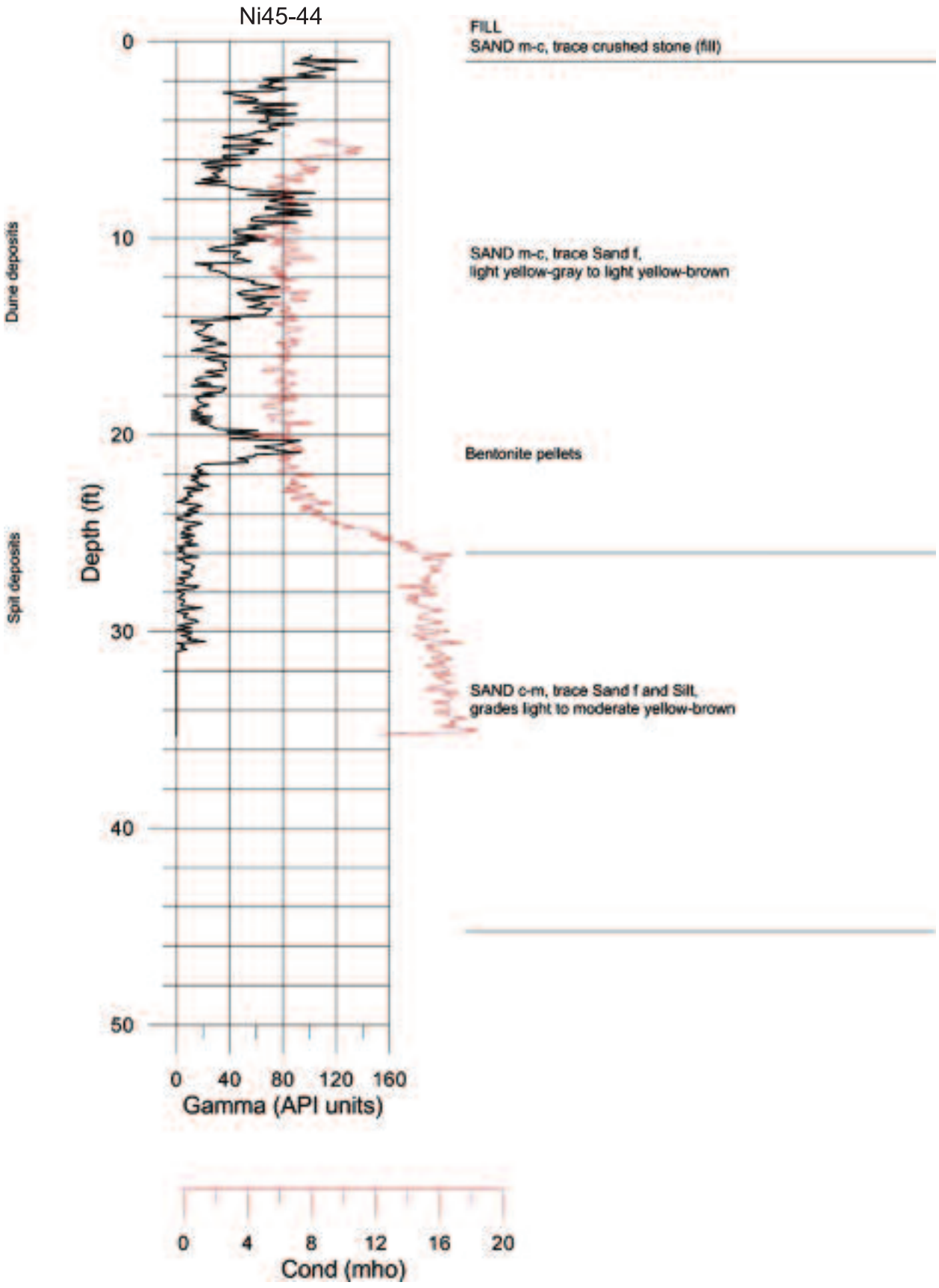

**APPENDIX A2.** Descriptive and geophysical logs for wells used in this study (continued).

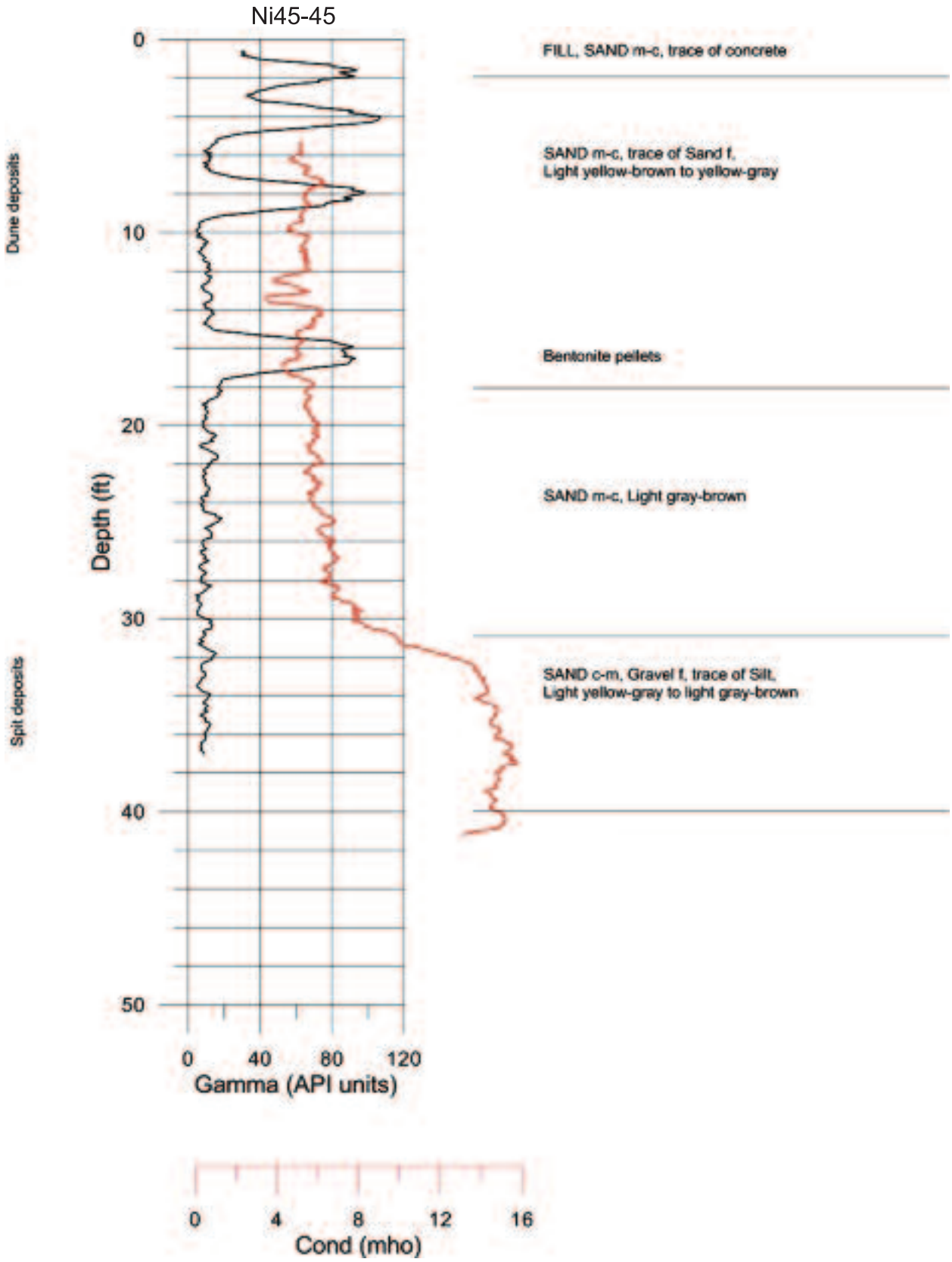

**APPENDIX A2.** Descriptive and geophysical logs for wells used in this study (continued).

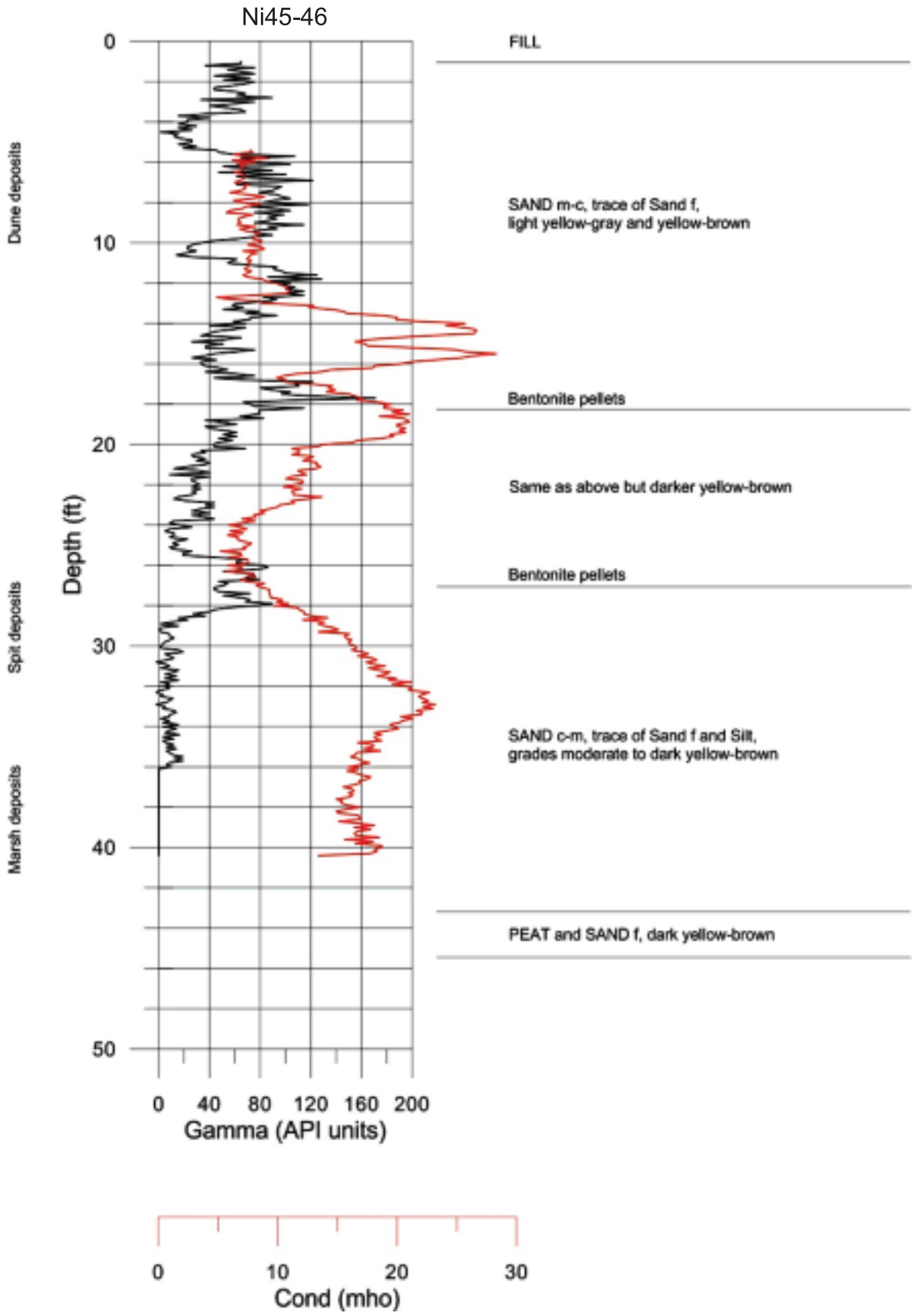

**APPENDIX A2.** Descriptive and geophysical logs for wells used in this study (continued).

**Log for well Ni45-38**

| Description | top | bottom |
|---|---|---|
| Leaf litter, twigs, Dk Brn to Dk Gry-Brn | 0 | 0.2 |
| Slt, Cly, carbonized plant fragments and roots, tr Sd f, color as above | 0.2 | 0.7 |
| SD m-f-c, Grvly f, tr Slt + roots; Med GRY N4 to N6; hydrogen sulfide odor | 0.7 | 1.5 |
| SD m-c-f, tr Grv + Slt; Med GRY-BRN 10YR5/2, hydrogen sulfide odor | 1.5 | 1.7 |
| As above, Light GRY to Light Y-BRN 10YR6/2 | 1.7 | 4.5 |

**Log for well Ni45-39**

| Description | top | bottom |
|---|---|---|
| Roots + duff | 0 | 0.3 |
| SD m-f-c; Light Y-GRY 10YR6/1 | 0.3 | 3.25 |
| SD m-c-f, Grvlly, f; Med GRY-BRN 10YR5/2 | 3.25 | 5.8 |

**Log for well Ni45-40**

| Description | top | bottom |
|---|---|---|
| Leaf litter, twigs, Dk Brn to Dk Gry-Brn | 0 | 0.35 |
| Slt, Cly, carbonized plant fragments and roots, tr Sd f, color as above | 0.35 | 1.25 |
| SD m-f-c, Grvly f, tr Slt + roots; Med GRY N4 to N6; hydrogen sulfide odor | 1.25 | 1.6 |
| SD m-c-f, tr Grv + Slt; Med BRN, hydrogen sulfide odor | 1.6 | 1.8 |
| As above, Light GRY to Light Y-BRN 10YR6/2 | 1.8 | 5.5 |

**Log for well Ni45-41**

| Description | top | bottom |
|---|---|---|
| Roots + duff, Sdy f-m | 0 | 0.2 |
| SD m-f-c; Light Y-GRY 10YR6/1 | 0.2 | 3.5 |
| SD m-c-f, Grvlly, f; Med GRY-BRN 10YR5/2 | 3.5 | 5.8 |

**Log for well Ni45-42**

| Description | top | bottom |
|---|---|---|
| Leaf litter, twigs, Dk Brn to Dk Gry-Brn | 0 | 0.3 |
| Slt, Cly, carbonized plant fragments and roots, tr Sd f, color as above | 0.3 | 1.5 |
| SD m-f-c, Grvly f, tr Slt + roots; Med GRY N4 to N6; hydrogen sulfide odor | 1.5 | 1.6 |
| SD m-c-f, tr Grv + Slt; Light GRY to Light Y-BRN 10YR6/2, hydrogen sulfide odor | 1.6 | 3.5 |

**Log for CMT wells Ni45-78 to Ni45-84**

| Description | top | bottom |
|---|---|---|
| ORG, tr Sd, f at top. SD, Org on bottom; V dusky Rd 10R 2/2 to dusky BRN 5YR 2/2 Leaves, twigs at top, Org. more decomposed w/ depth, bottom is Org.Slt. | 0 | 1.2 |
| SD, f-m (tr lams Sd, c), tr Org + Slt and charcoal; Pale BRN 5YR 2/2 | 1.2 | 2 |
| SD, f-m tr Org + Slt; GRY-BRN 5YR 3/2 to BRN-GRY 5YR 4/1 | 2 | 2.6 |
| SD, c-m, tr Org + Slt; 5YR 5/1 with burrows filled with SD f-m, and Org | 2.6 | 3 |
| SD, f-c tr Slt-Org, Mod BRN 5YR 4/4 | 3 | 4 |
| SD, f-m, tr Slt, sctrd charcoal grains, f; Mod BRN 5YR 4/4 | 4 | 5 |
| SD,m-f-c, tr Pbl, Grn, Slt; LT BRN-GRY 5YR 4/1, sctrd Fe-Ox stained grains; H2S odor | 5 | 7.5 |
| SD,m-c tr Pbl; LT BRN-GRY 5YR 4/1 | 7.5 | 8 |
| SD,m-f-c tr Slt; LT BRN-GRY 5YR 4/1 | 8 | 10.5 |

**APPENDIX B1.** Grain size data for samples from wells used in this study.

| Site Identifier | depth to top of sample (ft bls) | depth to bottom of sample (ft bls) | Median grain size (mm) | Mean grain size (mm) | Standard deviation | Skewness | Kurtosis | DGS Sample ID |
|---|---|---|---|---|---|---|---|---|
| Ni45-21 | 0 | 0.5 | 0.50 | 0.50 | 0.63 | 0.08 | 0.13 | 104557 |
| Ni45-21 | 0.5 | 0.65 | 0.40 | 0.42 | 0.67 | 0 | -0.05 | 104558 |
| Ni45-21 | 1.15 | 1.65 | 0.43 | 0.44 | 0.66 | 0.02 | 0.04 | 104560 |
| Ni45-21 | 0.65 | 1.15 | 0.43 | 0.44 | 0.67 | 0.03 | -0.08 | 104559 |
| Ni45-21 | 2.15 | 2.65 | 0.44 | 0.45 | 0.67 | 0.02 | 0.01 | 104562 |
| Ni45-21 | 1.65 | 2.15 | 0.42 | 0.43 | 0.67 | 0.01 | 0.08 | 104561 |
| Ni45-21 | 2.65 | 2.85 | 0.44 | 0.46 | 0.51 | 0.11 | -0.31 | 104563 |
| Ni45-21 | 4 | 4.5 | 0.42 | 0.44 | 0.66 | 0.07 | 0.26 | 104564 |
| Ni45-21 | 4.5 | 5.2 | 0.65 | 0.62 | 0.48 | 0.27 | -0.67 | 104565 |
| Ni45-21 | 5.7 | 6.2 | 0.43 | 0.44 | 0.70 | 0.05 | -0.45 | 104567 |
| Ni45-21 | 8.8 | 9.3 | 0.43 | 0.44 | 0.68 | 0.02 | -0.31 | 104569 |
| Ni45-21 | 10.3 | 10.8 | 0.41 | 0.42 | 0.69 | 0.04 | -0.29 | 104572 |
| Ni45-21 | 12.45 | 12.95 | 0.46 | 0.46 | 0.68 | 0.19 | -0.38 | 104574 |
| Ni45-21 | 13.95 | 14.45 | 0.41 | 0.42 | 0.71 | -0.06 | 0.03 | 104577 |
| Ni45-21 | 15.5 | 16 | 0.42 | 0.43 | 0.68 | 0.04 | -0.11 | 104580 |
| Ni45-21 | 17 | 17.5 | 0.38 | 0.39 | 0.73 | -0.18 | 1.26 | 104583 |
| Ni45-21 | 18.5 | 19 | 0.42 | 0.43 | 0.68 | 0.09 | 0.02 | 104586 |
| Ni45-21 | 20 | 20.5 | 0.43 | 0.44 | 0.68 | 0.06 | -0.25 | 104589 |
| Ni45-21 | 22 | 22.6 | 0.42 | 0.43 | 0.67 | -0.02 | -0.19 | 104592 |
| Ni45-21 | 23.7 | 24.2 | 0.45 | 0.46 | 0.69 | 0.18 | -0.7 | 104595 |
| Ni45-22 | 0 | 1 | 0.42 | 0.43 | 0.67 | 0.03 | -0.08 | 104597 |
| Ni45-22 | 1 | 1.5 | 0.42 | 0.43 | 0.67 | 0 | 0.24 | 104598 |
| Ni45-22 | 1.5 | 2 | 0.42 | 0.43 | 0.67 | -0.01 | -0.2 | 104599 |
| Ni45-22 | 2 | 2.5 | 0.43 | 0.44 | 0.68 | 0 | -0.18 | 104600 |
| Ni45-22 | 2.5 | 3 | 0.42 | 0.44 | 0.67 | 0.07 | -0.05 | 104601 |
| Ni45-22 | 3 | 3.5 | 0.42 | 0.44 | 0.69 | 0.01 | 0.01 | 104602 |
| Ni45-22 | 3.5 | 4 | 0.42 | 0.44 | 0.67 | 0.03 | -0.01 | 104603 |
| Ni45-22 | 4 | 4.45 | 0.43 | 0.45 | 0.67 | -0.08 | 0.18 | 104604 |
| Ni45-22 | 4.45 | 4.95 | 0.39 | 0.40 | 0.71 | -0.05 | 0.36 | 104605 |
| Ni45-22 | 5.95 | 6.25 | 0.42 | 0.43 | 0.67 | 0.03 | -0.06 | 104608 |
| Ni45-22 | 7.5 | 7.8 | 0.46 | 0.46 | 0.69 | 0.22 | -0.61 | 104611 |
| Ni45-22 | 9 | 9.5 | 0.41 | 0.43 | 0.69 | 0.01 | -0.08 | 104614 |
| Ni45-22 | 11.5 | 12 | 0.42 | 0.43 | 0.68 | 0.08 | -0.43 | 104617 |
| Ni45-22 | 13 | 13.5 | 0.44 | 0.45 | 0.70 | 0.13 | -0.64 | 104620 |
| Ni45-22 | 15.5 | 16 | 0.42 | 0.44 | 0.68 | -0.01 | 0.05 | 104622 |
| Ni45-22 | 17.5 | 18 | 0.35 | 0.34 | 0.79 | 0.24 | 6.64 | 104625 |
| Ni45-22 | 19.2 | 19.7 | 0.35 | 0.35 | 0.72 | -0.02 | 1.16 | 104627 |
| Ni45-22 | 21.4 | 21.9 | 0.33 | 0.33 | 0.72 | 0.01 | 0.74 | 104629 |
| Ni45-22 | 24 | 24.5 | 0.36 | 0.37 | 0.74 | -0.14 | 2.28 | 104631 |
| Ni45-22 | 25 | 25.5 | 0.41 | 0.42 | 0.67 | -0.03 | 0.12 | 104633 |

Note: ft bls - feet below land surface.

**APPENDIX B1.** Grain size data for samples from wells used in this study (continued).

| Site Identifier | depth to top of sample (ft bls) | depth to bottom of sample (ft bls) | Median grain size (mm) | Mean grain size (mm) | Standard deviation | Skewness | Kurtosis | DGS Sample ID |
|---|---|---|---|---|---|---|---|---|
| Ni45-23 | 0 | 1 | 0.42 | 0.43 | 0.69 | 0 | 0.1 | 104634 |
| Ni45-23 | 1 | 1.5 | 0.42 | 0.43 | 0.68 | 0.02 | -0.07 | 104635 |
| Ni45-23 | 1.5 | 2 | 0.43 | 0.45 | 0.67 | 0.04 | 0.21 | 104636 |
| Ni45-23 | 2 | 2.5 | 0.43 | 0.44 | 0.67 | 0.08 | -0.16 | 104637 |
| Ni45-23 | 2.5 | 3 | 0.42 | 0.44 | 0.70 | -0.02 | -0.12 | 104638 |
| Ni45-23 | 3 | 3.5 | 0.42 | 0.43 | 0.69 | 0.05 | -0.45 | 104639 |
| Ni45-23 | 3.8 | 4.3 | 0.44 | 0.45 | 0.70 | 0.01 | -0.31 | 104640 |
| Ni45-23 | 4.3 | 4.8 | 0.46 | 0.46 | 0.67 | 0.17 | -0.43 | 104641 |
| Ni45-24 | 0 | 0.5 | 0.44 | 0.46 | 0.66 | 0.05 | 0.26 | 104650 |
| Ni45-24 | 0.5 | 1 | 0.44 | 0.44 | 0.67 | 0.09 | 0.05 | 104651 |
| Ni45-24 | 1 | 1.5 | 0.43 | 0.44 | 0.68 | 0.04 | -0.06 | 104652 |
| Ni45-24 | 1.5 | 2 | 0.44 | 0.46 | 0.68 | 0.04 | -0.08 | 104653 |
| Ni45-24 | 2 | 2.5 | 0.41 | 0.43 | 0.67 | -0.07 | 0.12 | 104654 |
| Ni45-24 | 2.5 | 2.8 | 0.42 | 0.44 | 0.69 | -0.05 | 0.03 | 104655 |
| Ni45-24 | 3.8 | 4.3 | 0.41 | 0.42 | 0.70 | -0.07 | 0.06 | 104656 |
| Ni45-24 | 4.3 | 4.8 | 0.43 | 0.44 | 0.67 | 0.01 | -0.11 | 104657 |
| Ni45-25 | 0 | 0.5 | 0.49 | 0.49 | 0.68 | 0.19 | -0.09 | 104667 |
| Ni45-25 | 0.5 | 1 | 0.44 | 0.45 | 0.67 | 0.04 | 0.08 | 104668 |
| Ni45-25 | 1 | 1.4 | 0.43 | 0.44 | 0.68 | 0.01 | 0 | 104669 |
| Ni45-25 | 1.4 | 1.8 | 0.42 | 0.43 | 0.67 | 0.03 | 0.03 | 104670 |
| Ni45-25 | 1.8 | 2.2 | 0.44 | 0.47 | 0.62 | -0.05 | 0.41 | 104671 |
| Ni45-25 | 2.2 | 2.7 | 0.46 | 0.49 | 0.56 | 0.04 | 0.05 | 104672 |
| Ni45-25 | 3.5 | 4 | 0.47 | 0.49 | 0.61 | -0.03 | 0.09 | 104673 |
| Ni45-25 | 4 | 4.5 | 0.52 | 0.52 | 0.61 | 0.03 | 0.11 | 104674 |
| Ni45-25 | 4.5 | 5 | 0.48 | 0.49 | 0.61 | 0.05 | 0.25 | 104675 |
| Ni45-26 | 0 | 0.3 | 0.43 | 0.44 | 0.66 | -0.02 | 0.27 | 104685 |
| Ni45-26 | 0.3 | 0.6 | 0.42 | 0.44 | 0.67 | 0.01 | 0.13 | 104686 |
| Ni45-26 | 0.6 | 1.1 | 0.41 | 0.43 | 0.69 | 0.02 | -0.01 | 104687 |
| Ni45-26 | 1.1 | 1.6 | 0.47 | 0.47 | 0.66 | 0.16 | -0.14 | 104688 |
| Ni45-26 | 1.6 | 2.1 | 0.48 | 0.48 | 0.66 | 0.12 | -0.14 | 104689 |
| Ni45-26 | 2.1 | 2.6 | 0.42 | 0.44 | 0.67 | 0 | 0.14 | 104690 |
| Ni45-26 | 3.5 | 3.9 | 0.40 | 0.41 | 0.70 | -0.07 | 0.54 | 104691 |
| Ni45-26 | 3.9 | 4.4 | 0.44 | 0.45 | 0.66 | 0.06 | 0.22 | 104692 |
| Ni45-26 | 4.4 | 4.9 | 0.43 | 0.45 | 0.68 | 0.03 | -0.03 | 104693 |

Note: ft bls - feet below land surface.

**APPENDIX B1.** Grain size data for samples from wells used in this study (continued).

| Site identifier | depth to top of sample (ft bls) | depth to bottom of sample (ft bls) | Median grain size (mm) | Mean grain size (mm) | Standard deviation | Skewness | Kurtosis | DGS Sample ID |
|---|---|---|---|---|---|---|---|---|
| Ni45-27 | 0 | 0.5 | 0.44 | 0.46 | 0.67 | 0.03 | -0.09 | 104703 |
| Ni45-27 | 0.5 | 1 | 0.44 | 0.45 | 0.67 | 0.07 | -0.02 | 104704 |
| Ni45-27 | 1 | 1.5 | 0.44 | 0.46 | 0.68 | 0.06 | -0.06 | 104705 |
| Ni45-27 | 1.5 | 2 | 0.44 | 0.44 | 0.66 | 0.05 | 0.01 | 104706 |
| Ni45-27 | 2 | 2.5 | 0.41 | 0.43 | 0.67 | -0.12 | 0.35 | 104707 |
| Ni45-27 | 3.5 | 4 | 0.41 | 0.41 | 0.68 | 0.05 | -0.34 | 104708 |
| Ni45-27 | 4 | 4.5 | 0.41 | 0.42 | 0.69 | 0.01 | -0.08 | 104709 |
| Ni45-27 | 4.5 | 5 | 0.39 | 0.41 | 0.69 | -0.1 | 0.39 | 104710 |
| Ni45-28 | 0 | 0.5 | 0.42 | 0.44 | 0.68 | 0.06 | -0.06 | 104717 |
| Ni45-28 | 0.5 | 1 | 0.43 | 0.44 | 0.69 | 0.05 | -0.16 | 104718 |
| Ni45-28 | 1 | 1.5 | 0.48 | 0.48 | 0.68 | 0.23 | -0.44 | 104719 |
| Ni45-28 | 1.5 | 2 | 0.53 | 0.50 | 0.66 | 0.27 | 0.11 | 104720 |
| Ni45-28 | 2 | 2.5 | 0.44 | 0.46 | 0.69 | 0.03 | -0.39 | 104721 |
| Ni45-28 | 2.5 | 2.9 | 0.46 | 0.47 | 0.69 | 0.09 | -0.37 | 104722 |
| Ni45-28 | 3.5 | 4 | 0.49 | 0.48 | 0.67 | 0.21 | -0.03 | 104723 |
| Ni45-28 | 4 | 4.5 | 0.47 | 0.47 | 0.68 | 0.16 | -0.49 | 104724 |
| Ni45-28 | 4.5 | 5 | 0.43 | 0.45 | 0.68 | 0 | 0.01 | 104725 |
| Ni45-29 | 0 | 0.5 | 0.41 | 0.43 | 0.71 | -0.18 | 0.37 | 104736 |
| Ni45-29 | 0.5 | 1 | 0.41 | 0.43 | 0.70 | -0.04 | 0.02 | 104737 |
| Ni45-29 | 1 | 1.5 | 0.42 | 0.44 | 0.71 | -0.03 | -0.18 | 104738 |
| Ni45-29 | 1.5 | 2 | 0.47 | 0.47 | 0.65 | 0.02 | -0.13 | 104739 |

Note: ft bls - feet below land surface.

**APPENDIX B2.** Porosity and moisture content data for samples from wells used in this study.

| Site Identifier | Sample ID | sample top (ft bls) | sample bottom (ft bls) | n | Vw |
|---|---|---|---|---|---|
| Ni45-68 | 105322 | 0 | 1.5 | 43.6 | 0.62 |
| | 105323 | 1.5 | 2.8 | 43.5 | 3.37 |
| | 105324 | 2.8 | 3.35 | 43.2 | 2.24 |
| | 105325 | 3.35 | 4.5 | 45.5 | 4.66 |
| | 105326 | 4.5 | 5.2 | 40.6 | 1.12 |
| | 105327 | 5.2 | 5.8 | 47.0 | 4.05 |
| | 105328 | 5.8 | 6 | 51.0 | 1.47 |
| | | | | | |
| Ni45-69 | 105329 | 0 | 1.5 | 48.3 | 1.51 |
| | 105330 | 1.5 | 3 | 43.3 | 2.71 |
| | 105331 | 3 | 4.5 | 42.8 | 3.72 |
| | 105332 | 4.5 | 6 | 44.9 | 4.71 |
| | 105333 | 6 | 7 | 40.3 | 4.44 |
| | | | | | |
| Ni45-70 | 105334 | 0 | 1 | 38.1 | 2.07 |
| | 105335 | 1 | 2 | 44.3 | 3.10 |
| | 105336 | 2 | 3 | 41.1 | 3.94 |
| | 105337 | 3 | 4 | 45.5 | 3.34 |
| | 105338 | 4 | 5 | 40.3 | 4.21 |
| | 105339 | 5 | 6 | 44.7 | 5.01 |
| | 105340 | 6 | 7 | 44.2 | 3.97 |
| | 105341 | 7 | 8 | 45.5 | 3.78 |
| | | | | | |
| Ni45-71 | 105342 | 0 | 1 | 41.3 | 13.19 |
| | 105343 | 1 | 1.7 | 26.3 | 10.22 |
| | 105344 | 1.7 | 2.5 | 37.3 | 9.32 |
| | 105345 | 2.5 | 4.25 | 43.3 | 9.63 |
| | 105346 | 4.25 | 5.4 | 42.5 | 8.53 |
| | 105347 | 5.4 | 6.35 | 38.8 | 11.03 |
| | 105348 | 6.35 | 7.35 | 46.1 | 9.38 |
| | 105349 | 7.35 | 8.35 | 38.5 | 9.38 |
| | | | | | |
| Ni45-72 | 105350 | 0 | 1 | 43.1 | 5.86 |
| | 105351 | 1 | 2 | 38.2 | 5.01 |
| | 105352 | 2 | 3 | 44.9 | 5.28 |
| | 105353 | 3 | 4 | 43.0 | 5.33 |
| | 105354 | 4 | 5 | 42.8 | 10.10 |
| | 105355 | 5 | 6 | 43.9 | 6.59 |
| | 105356 | 6 | 7 | 39.7 | 6.48 |

Note: ft bls – feet below land surface
n – porosity
Vw - estimate of volumetric water content

**APPENDIX B2.** Porosity and moisture content data for samples from wells used in this study (continued).

| Site Identifier | Sample ID | sample top (ft bls) | sample bottom (ft bls) | n | Vw |
|---|---|---|---|---|---|
| Ni45-73 | 105358 | 0 | 1 | 46.3 | 6.17 |
| | 105359 | 1 | 2 | 38.9 | 4.35 |
| | 105360 | 2 | 3 | 38.7 | 7.61 |
| | 105361 | 3 | 4 | 40.5 | 6.14 |
| | 105362 | 4 | 5 | 41.8 | 5.44 |
| | 105363 | 5 | 6 | 40.5 | 6.22 |
| | 105364 | 6 | 7 | 41.1 | 5.82 |
| | | | | | |
| Ni45-74 | 105367 | 0 | 1 | 49.2 | 3.25 |
| | 105368 | 1 | 2 | 48.2 | 2.84 |
| | 105369 | 2 | 3 | 38.5 | 4.64 |
| | 105370 | 3 | 4 | 39.8 | 5.03 |
| | 105371 | 4 | 5 | 38.8 | 6.86 |
| | 105372 | 5 | 6 | 38.8 | 5.66 |
| | 105373 | 6 | 7 | 36.9 | 5.58 |
| | | | | | |
| Ni45-76 | 105375 | 0 | 1 | 48.6 | 2.08 |
| | 105376 | 1 | 2 | 48.7 | 4.32 |
| | 105377 | 2 | 3 | 44.0 | 5.64 |
| | 105378 | 3 | 4 | 46.0 | 5.44 |
| | 105379 | 4 | 5 | 46.7 | 8.67 |
| | 105380 | 5 | 6 | 45.2 | 9.11 |
| | 105381 | 6 | 7 | 44.8 | 7.91 |
| | | | | | |
| Ni45-75 | 105383 | 0 | 1 | 60.2 | 5.18 |
| | 105384 | 1 | 2 | 43.4 | 5.08 |
| | 105385 | 2 | 3 | 33.0 | 6.40 |
| | 105386 | 3 | 4 | 41.5 | 5.47 |
| | 105387 | 4 | 5 | 46.3 | 5.36 |
| | 105388 | 5 | 6 | 49.0 | 4.87 |
| | 105389 | 6 | 7 | 48.1 | 4.38 |
| | | | | | |
| Ni45-77 | 105392 | 0 | 1 | 54.1 | 6.83 |
| | 105393 | 1 | 2 | 46.3 | 4.46 |
| | 105394 | 2 | 3 | 45.5 | 4.59 |
| | 105395 | 3 | 4 | 44.9 | 5.69 |
| | 105396 | 4 | 5 | 44.5 | 4.58 |
| | 105397 | 5 | 6 | 47.0 | 4.79 |
| | 105398 | 6 | 7 | 46.4 | 5.48 |

Note: ft bls – feet below land surface
n – porosity
Vw - estimate of volumetric water content

**APPENDIX C.** Slug test results for wells used in this study.

| DGS Identifier | K | Number of observations |
|---|---|---|
| Ni45-33 | 150 | 3 |
| Ni45-35 | 176 | 3 |
| Ni45-36 | 179 | 3 |
| Ni45-37 | 133 | 3 |
| Ni45-38 | 49 | 5 |
| Ni45-39 | 20 | 3 |
| Ni45-40 | 40 | 4 |
| Ni45-41 | 11 | 3 |
| Ni45-42 | 6 | 3 |
| Ni45-43 | 123 | 3 |
| Ni45-44 | 133 | 3 |
| Ni45-45 | 127 | 3 |
| Ni45-46 | 103 | 3 |
| Ni44-16 | 70 | 2 |
| Ni45-15 | 49 | 3 |
| Ni45-16 | 22 | 3 |
| Ni45-17 | 55 | 4 |

Note: K - average hydraulic conductivity (feet per day) for the number of observations.

**APPENDIX D**. Time series plots of daily mean and manually measured depth to water and daily mean temperature for selected wells at Cape Henlopen State Park. Mean daily groundwater levels and temperatures were calculated as average of 15-minute measurements recorded with a datalogging pressure transducer-thermistor instrument. dtw – depth to water; temp - temperature

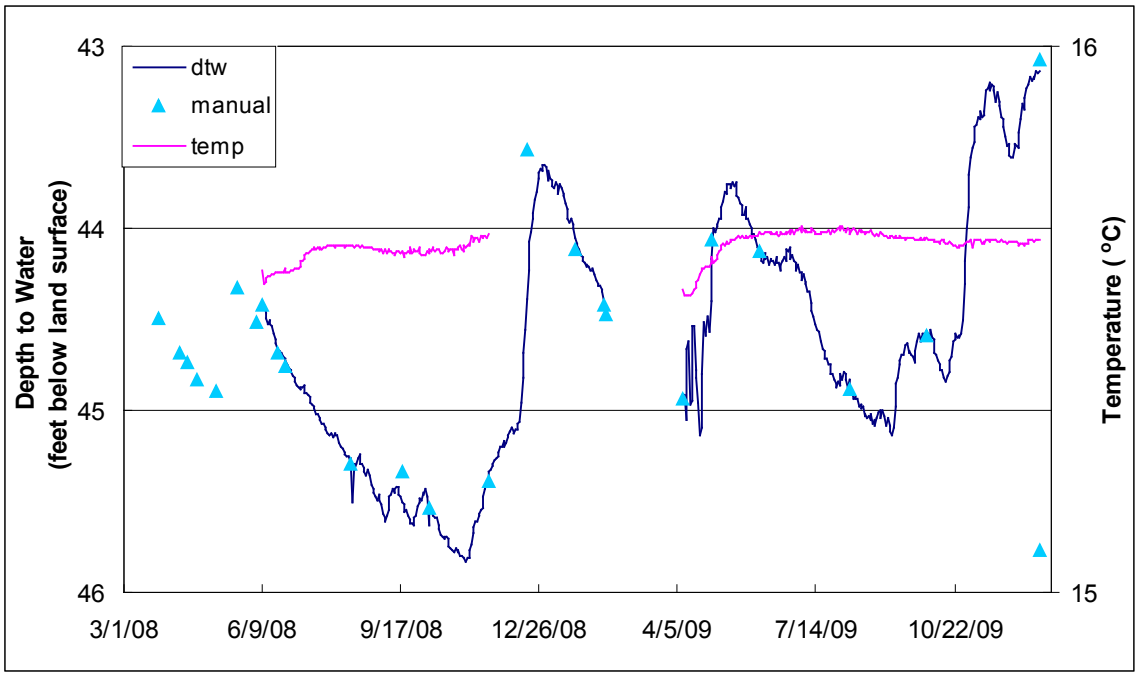


**Figure D1.** Measurements for well Ni45-33.

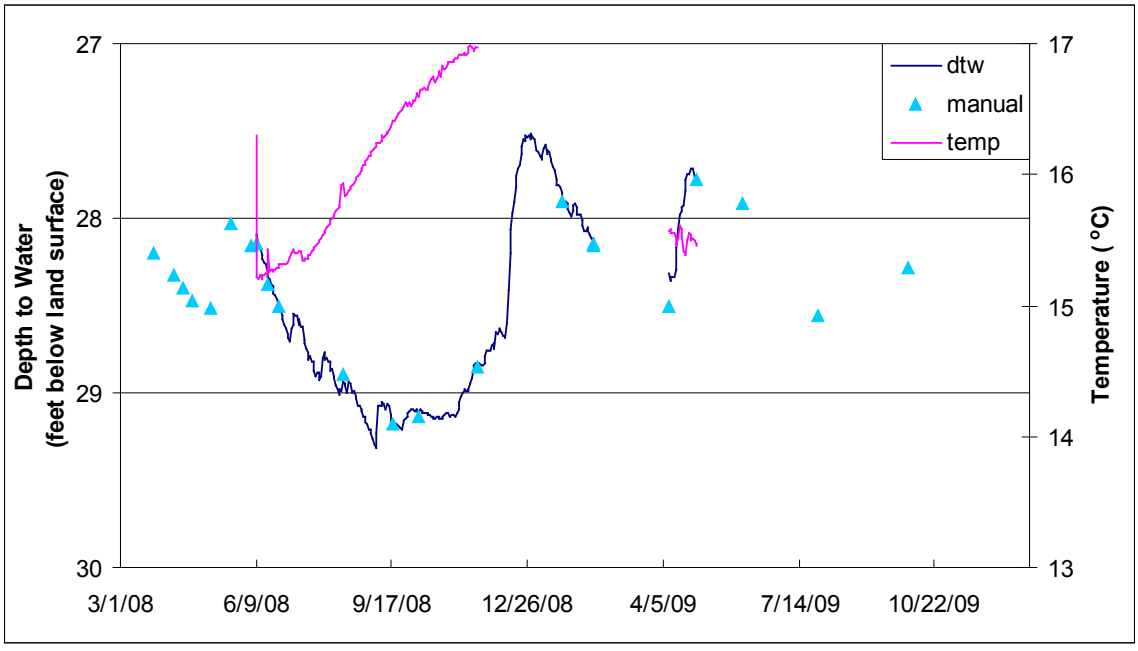


**Figure D2.** Measurements for well Ni45-34.

**APPENDIX D**. Time series plots of daily mean and manually measured depth to water and daily mean temperature for selected wells at Cape Henlopen State Park (continued). Mean daily groundwater levels and temperatures were calculated as average of 15-minute measurements recorded with a datalogging pressure transducer-thermistor instrument. dtw – depth to water; temp - temperature

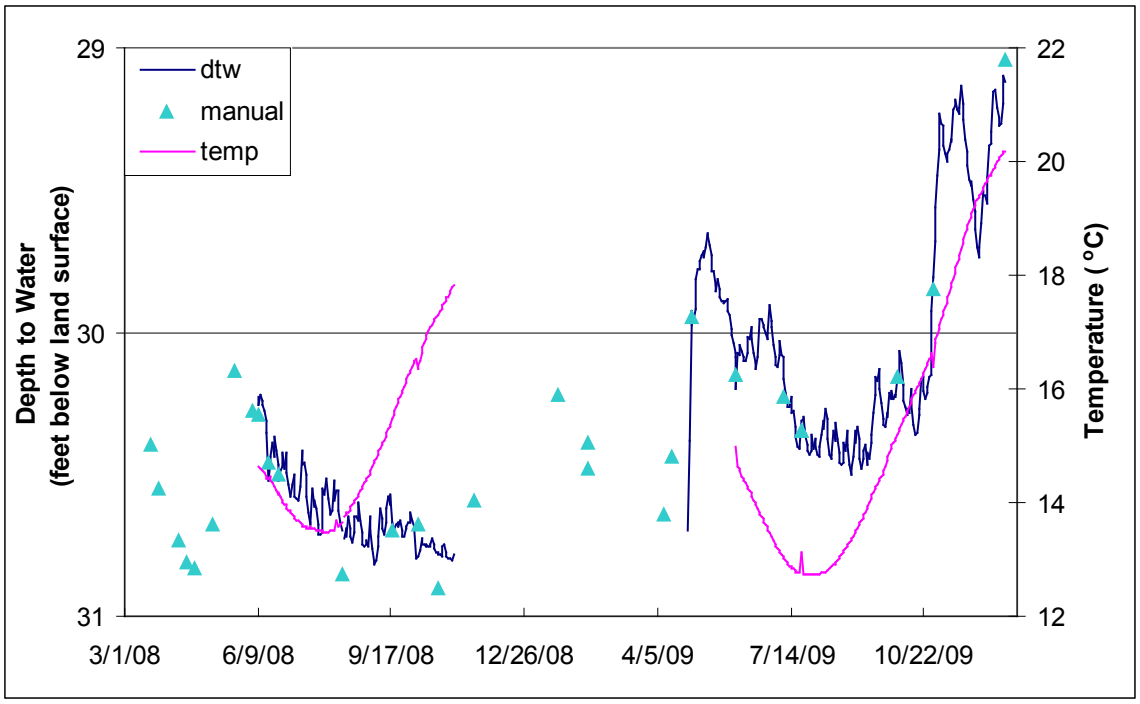


**Figure D3.** Measurements for well Ni45-35.

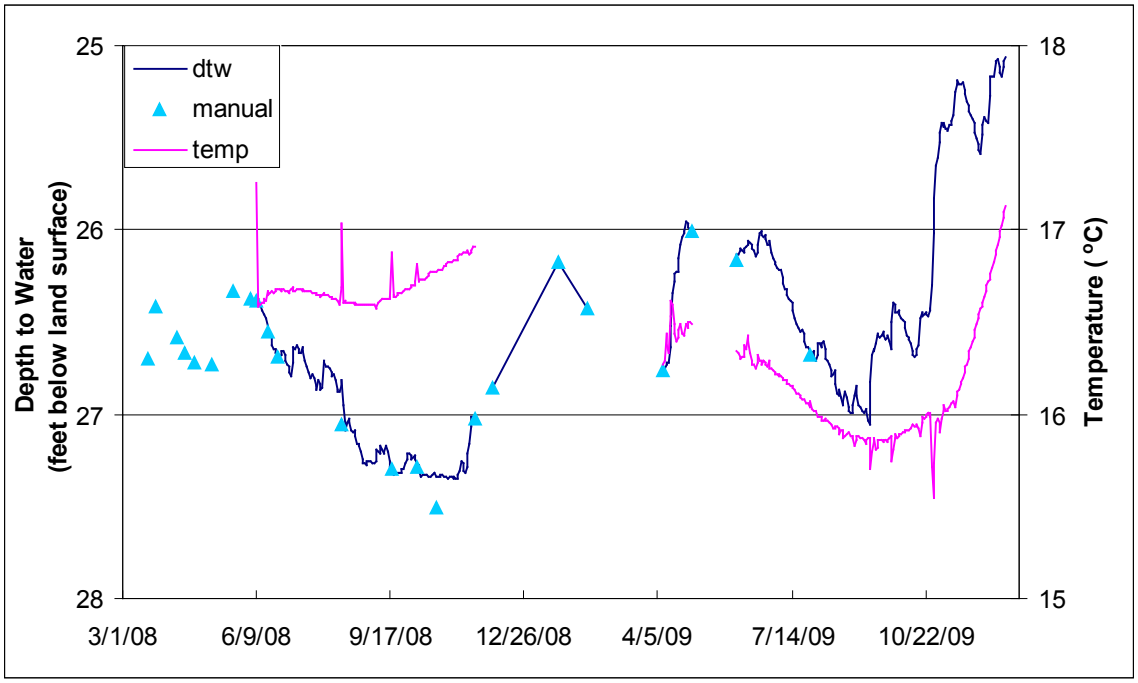


**Figure D4.** Measurements for well Ni45-36.

**APPENDIX D**. Time series plots of daily mean and manually measured depth to water and daily mean temperature for selected wells at Cape Henlopen State Park (continued). Mean daily groundwater levels and temperatures were calculated as average of 15-minute measurements recorded with a datalogging pressure transducer-thermistor instrument. dtw – depth to water; temp - temperature

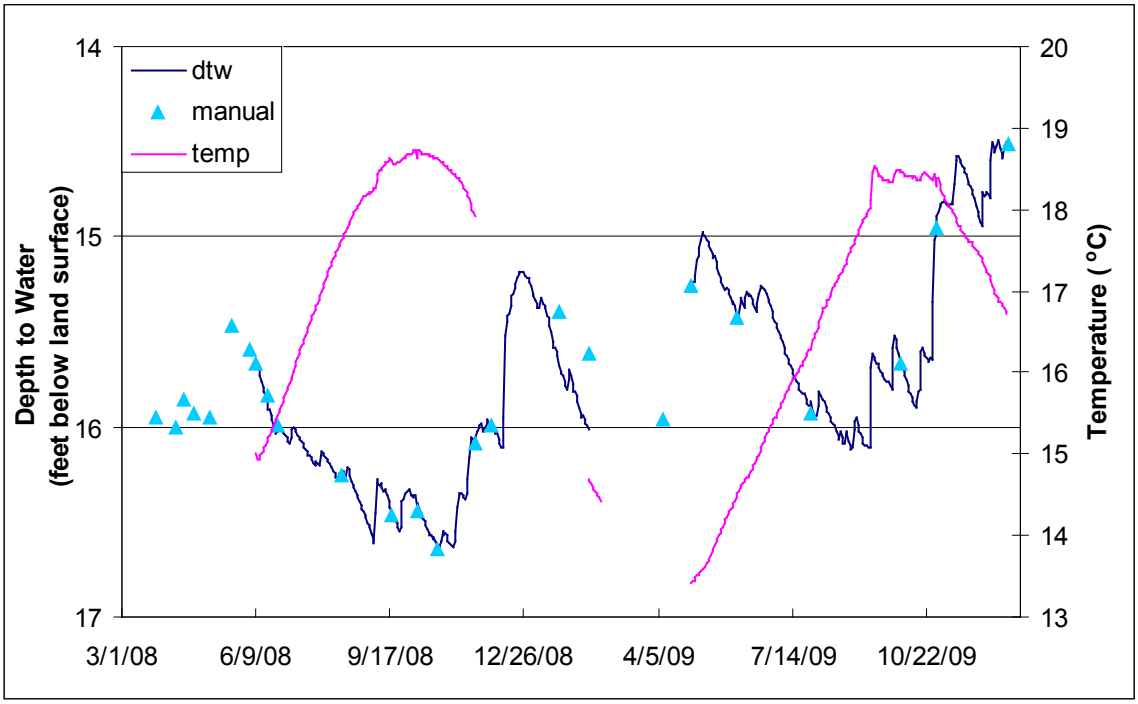


**Figure D5.** Measurements for well Ni45-37.

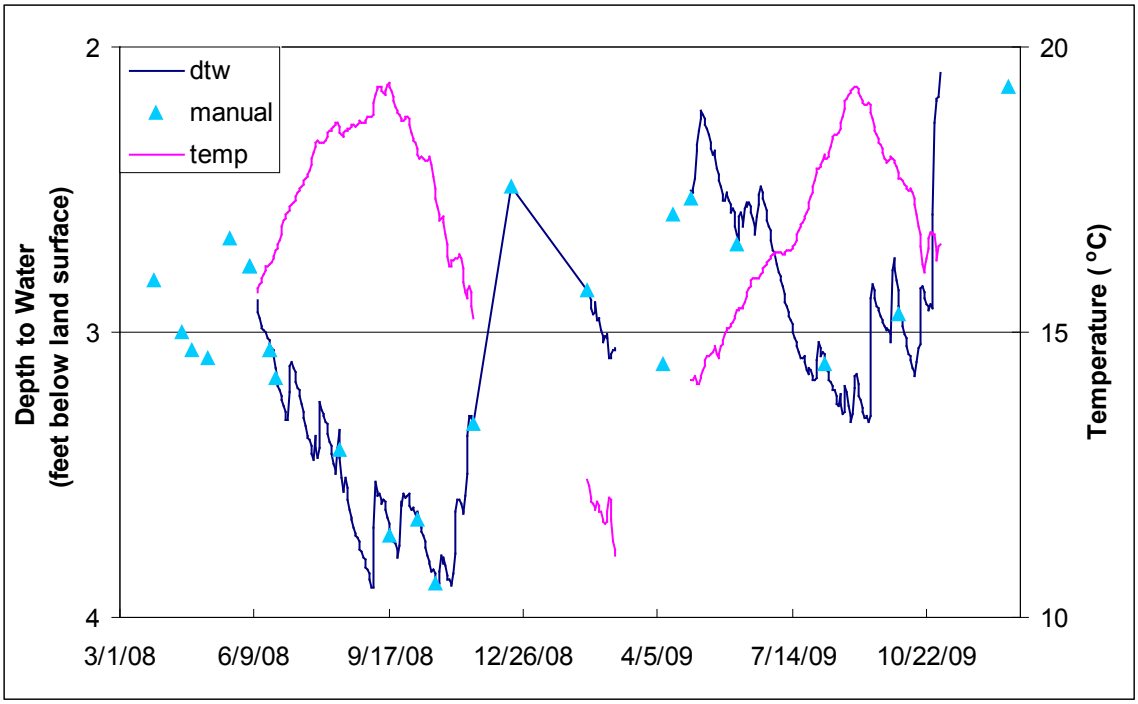


**Figure D6.** Measurements for well Ni45-42.

**APPENDIX D**. Time series plots of daily mean and manually measured depth to water and daily mean temperature for selected wells at Cape Henlopen State Park (continued). Mean daily groundwater levels and temperatures were calculated as average of 15-minute measurements recorded with a datalogging pressure transducer-thermistor instrument. dtw – depth to water; temp - temperature

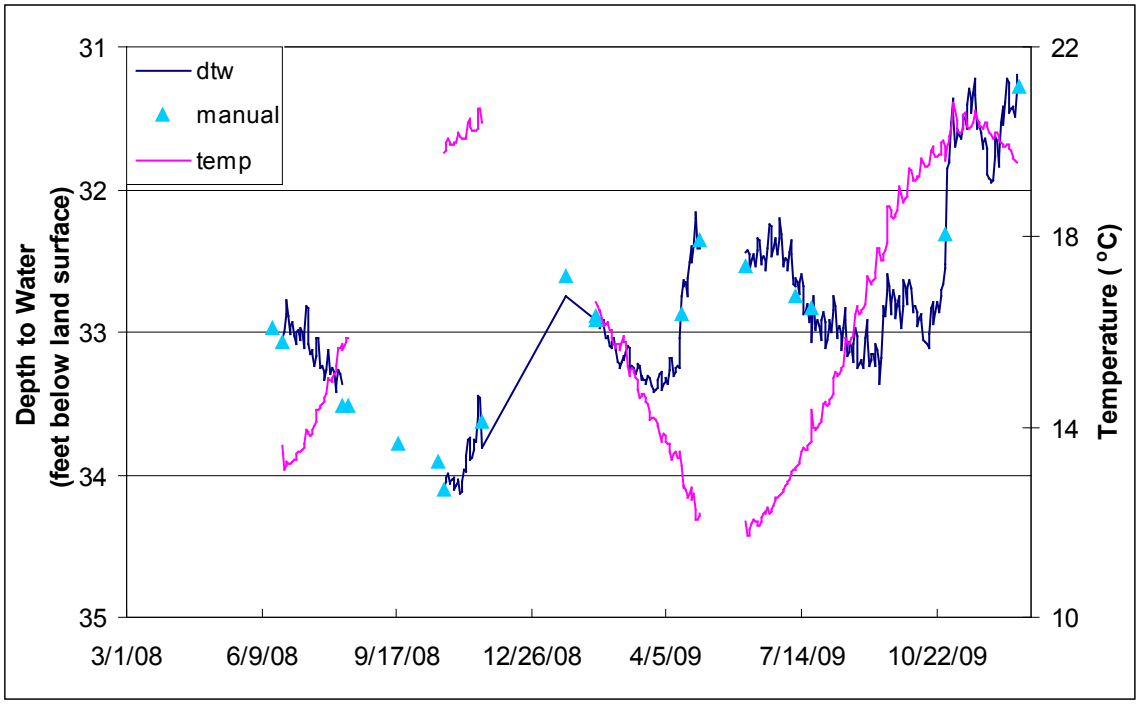


**Figure D7.** Measurements for well Ni45-43.

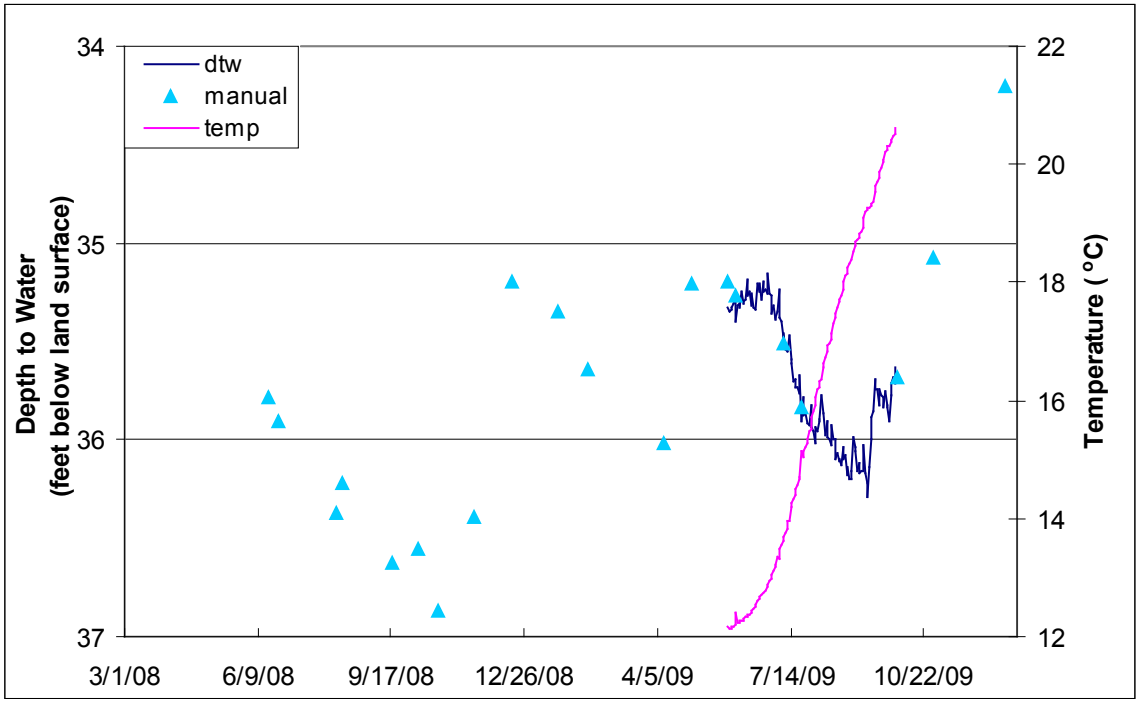


**Figure D8.** Measurements for well Ni45-44.

**APPENDIX D**. Time series plots of daily mean and manually measured depth to water and daily mean temperature for selected wells at Cape Henlopen State Park (continued). Mean daily groundwater levels and temperatures were calculated as average of 15-minute measurements recorded with a datalogging pressure transducer-thermistor instrument. dtw – depth to water; temp - temperature

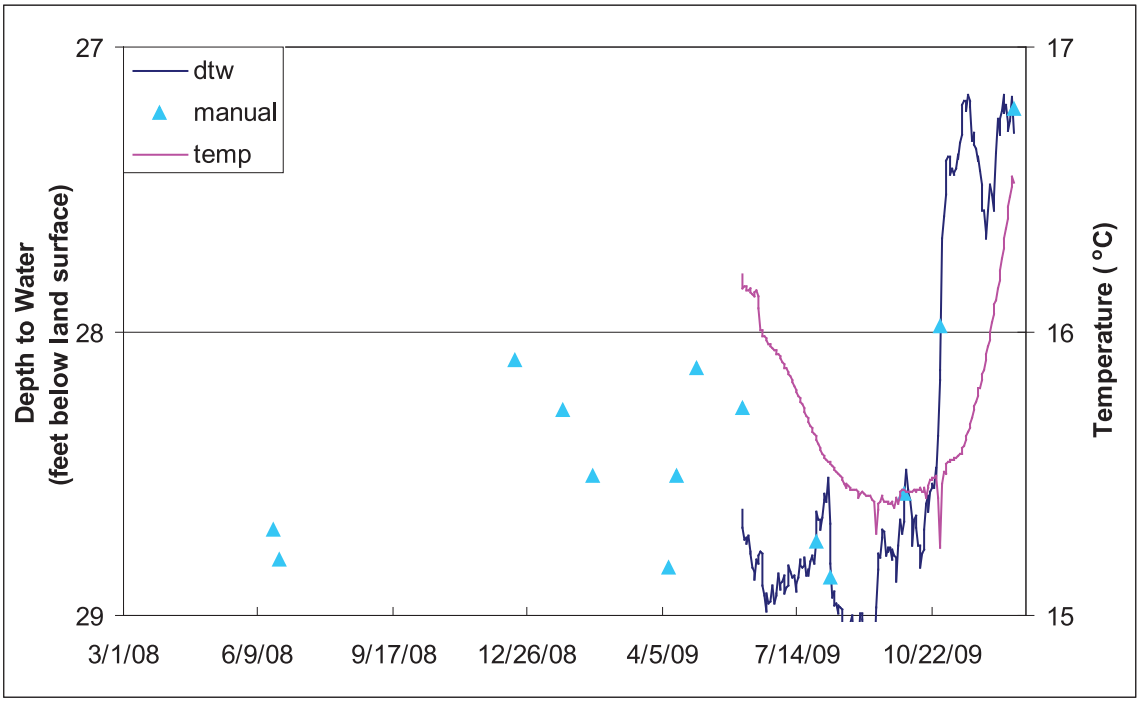


**Figure D9.** Measurements for well Ni45-45.

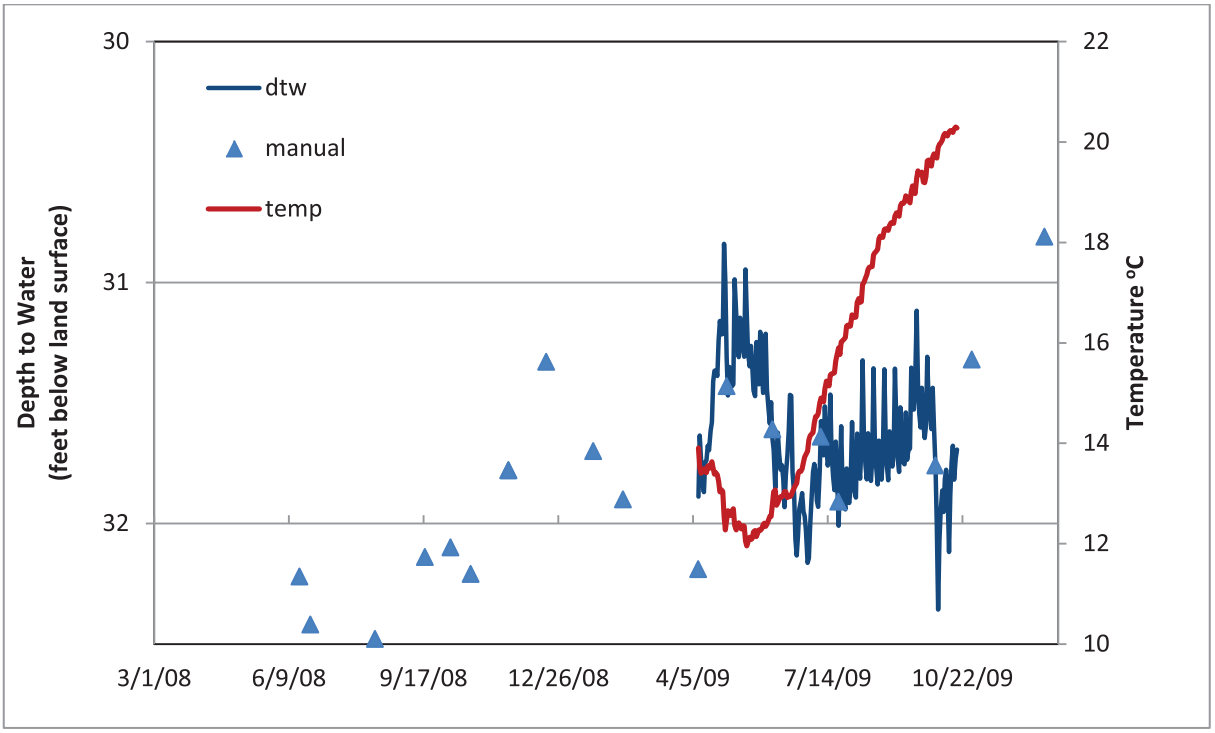


**Figure D10.** Measurements for well Ni45-46.

**APPENDIX D**. Time series plots of daily mean and manually measured depth to water and daily mean temperature for selected wells at Cape Henlopen State Park (continued). Mean daily groundwater levels and temperatures were calculated as average of 15-minute measurements recorded with a datalogging pressure transducer-thermistor instrument. dtw – depth to water; temp - temperature

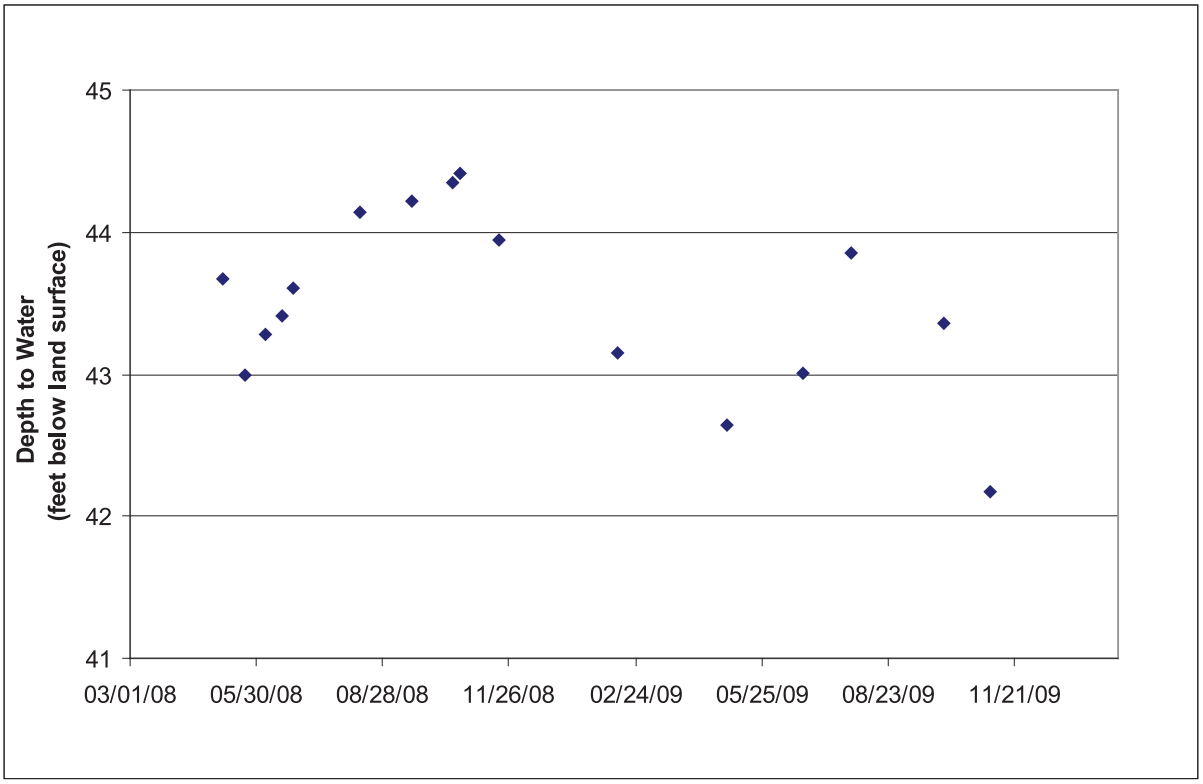


**Figure D11.** Manually measured depth to water for well Ni44-16.

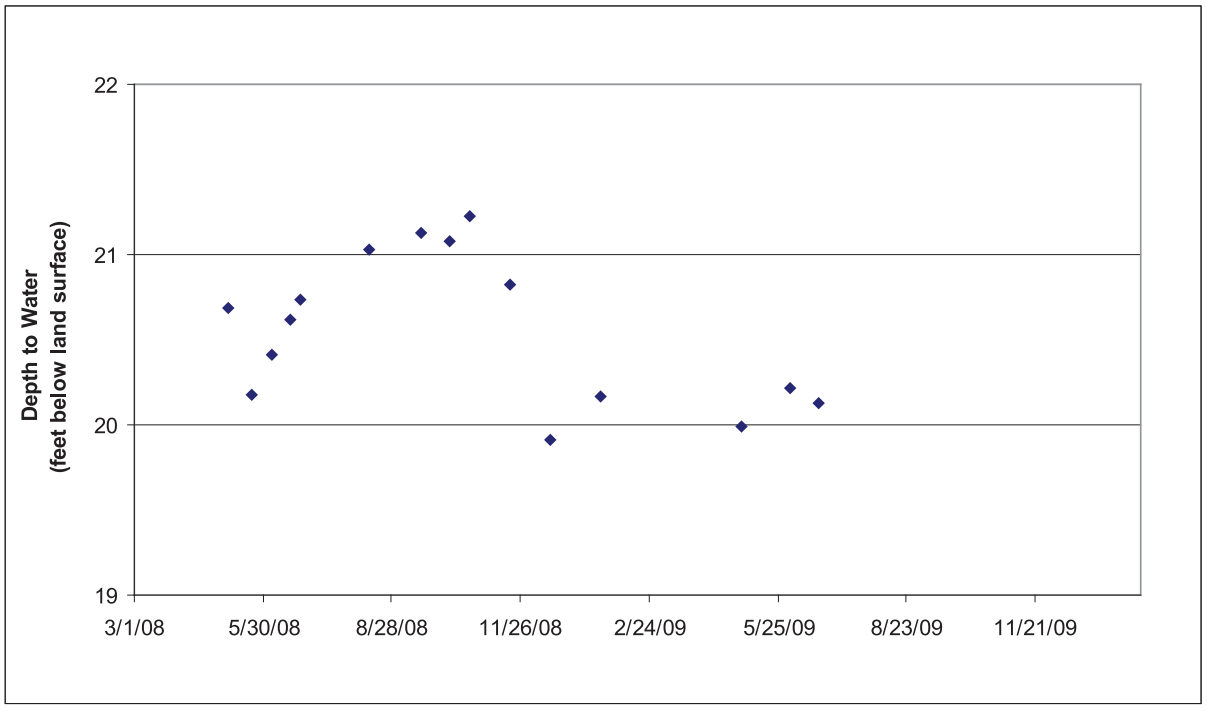


**Figure D12.** Manually measured depth to water for well Ni45-15.

**APPENDIX D**. Time series plots of daily mean and manually measured depth to water and daily mean temperature for selected wells at Cape Henlopen State Park (continued). Mean daily groundwater levels and temperatures were calculated as average of 15-minute measurements recorded with a datalogging pressure transducer-thermistor instrument. dtw – depth to water; temp – temperature

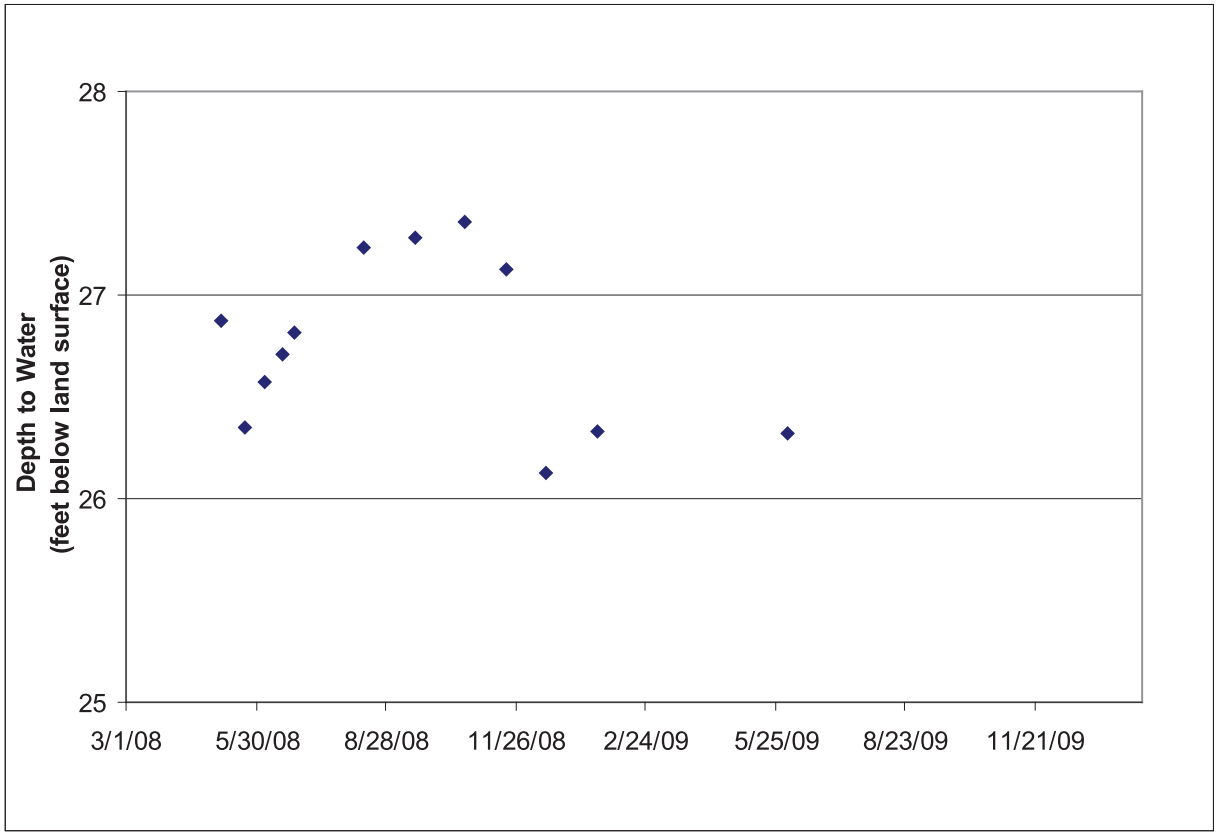


**Figure D13.** Manually measured depth to water for well Ni45-16.

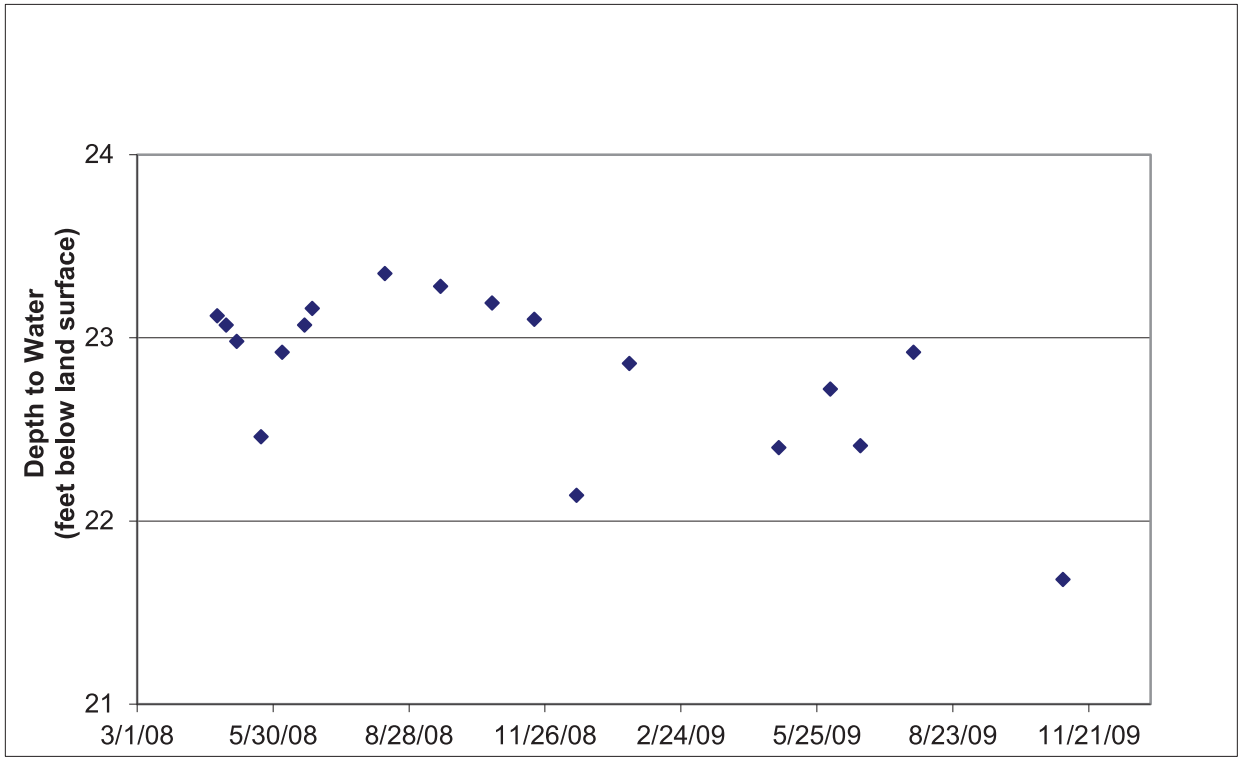


**Figure D14.** Manually measured depth to water for well Ni45-17.

**APPENDIX D**. Time series plots of daily mean and manually measured depth to water and daily mean temperature for selected wells at Cape Henlopen State Park (continued). Mean daily groundwater levels and temperatures were calculated as average of 15-minute measurements recorded with a datalogging pressure transducer-thermistor instrument. dtw – depth to water; temp - temperature

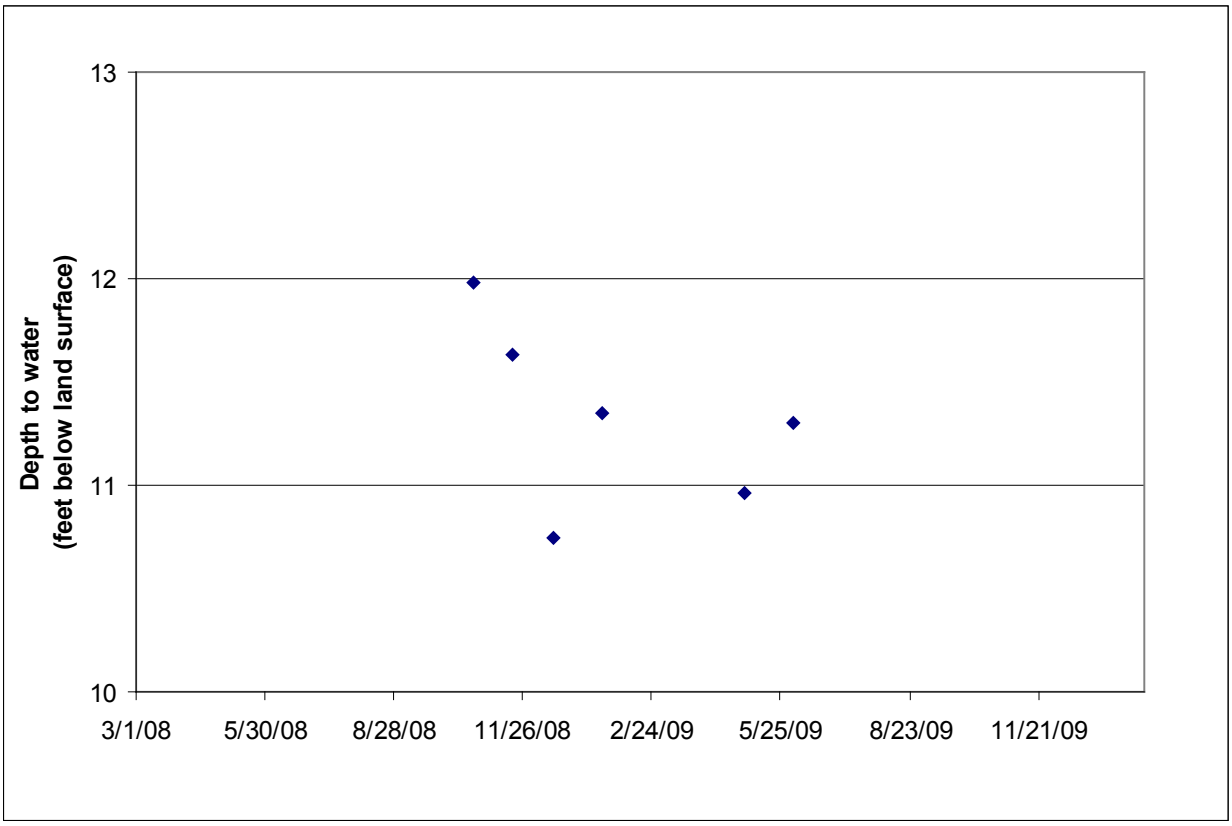


**Figure D15.** Manually measured depth to water for well Ni45-18.

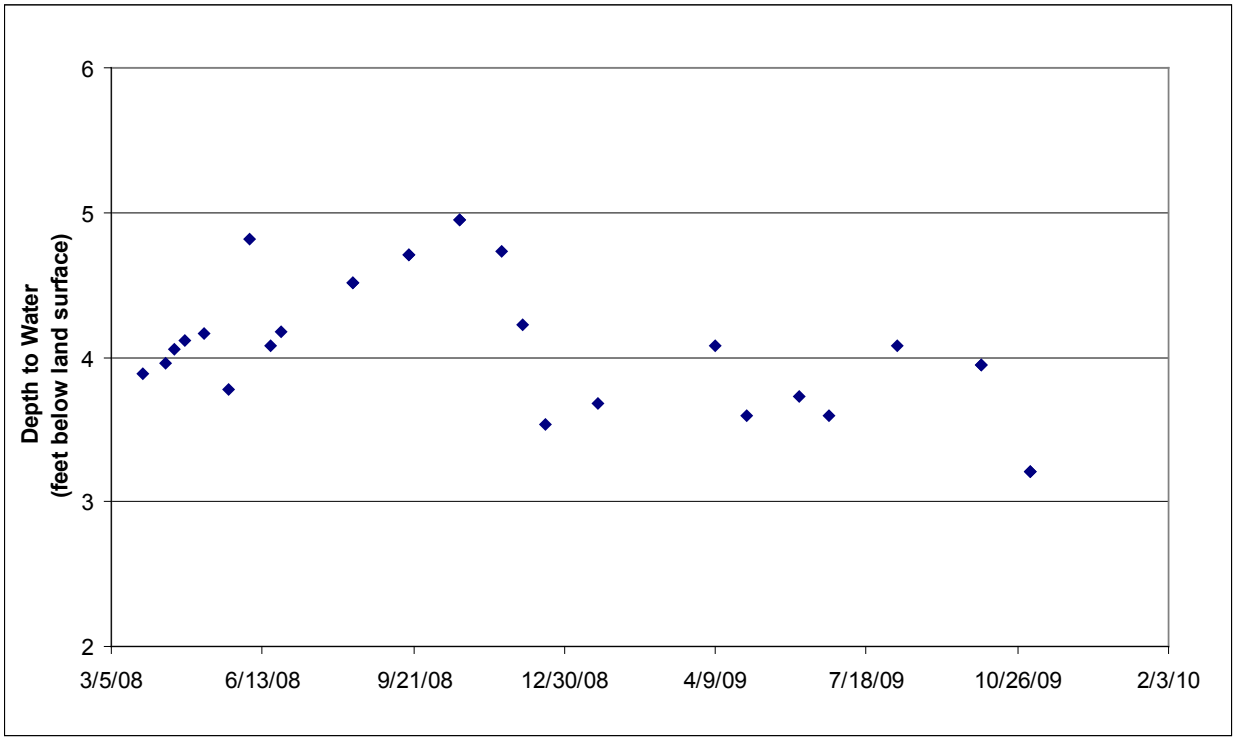


**Figure D16.** Manually measured depth to water for well Ni45-38.

**APPENDIX D**. Time series plots of daily mean and manually measured depth to water and daily mean temperature for selected wells at Cape Henlopen State Park (continued). Mean daily groundwater levels and temperatures were calculated as average of 15-minute measurements recorded with a datalogging pressure transducer-thermistor instrument. dtw – depth to water; temp - temperature

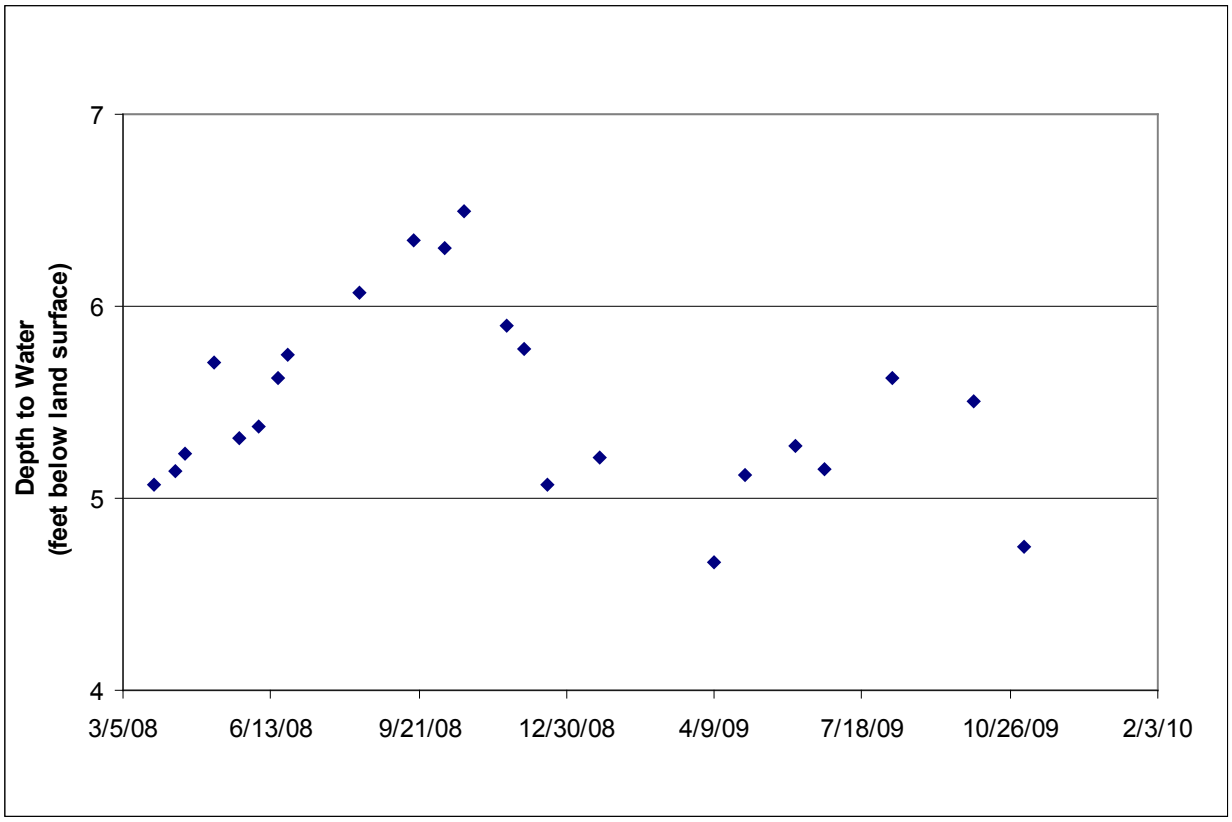


**Figure D17.** Manually measured depth to water for well Ni45-39.

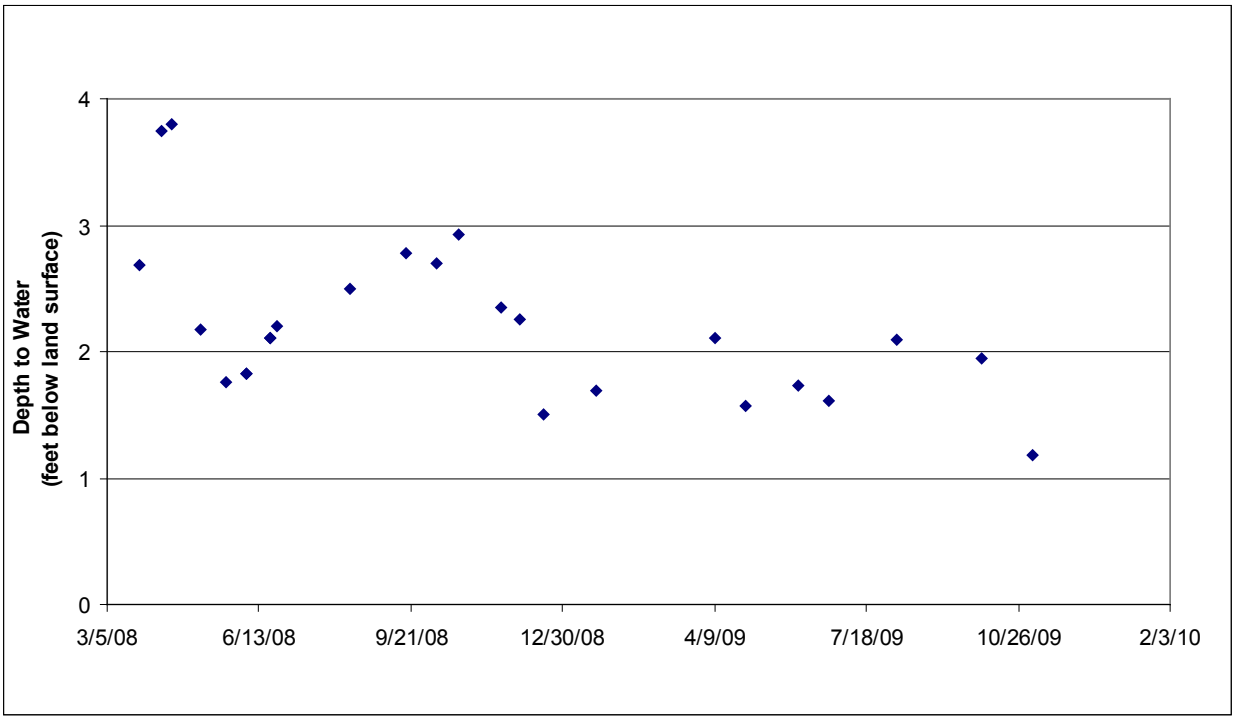


**Figure D18.** Manually measured depth to water for well Ni45-40.

**APPENDIX D**. Time series plots of daily mean and manually measured depth to water and daily mean temperature for selected wells at Cape Henlopen State Park (continued). Mean daily groundwater levels and temperatures were calculated as average of 15-minute measurements recorded with a datalogging pressure transducer-thermistor instrument. dtw – depth to water; temp - temperature

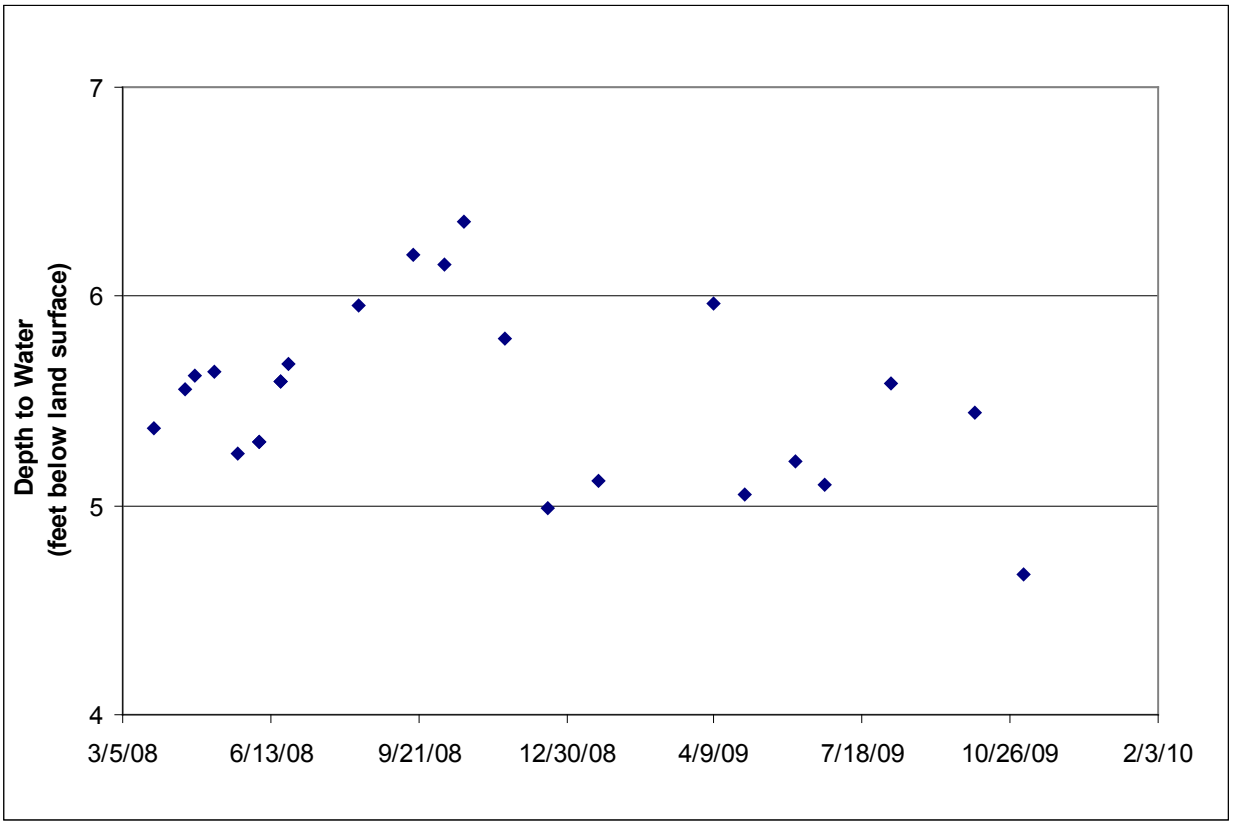


**Figure D19.** Manually measured depth to water for well Ni45-41.


Delaware Geological Survey
University of Delaware
Newark, Delaware 19716